NAVAL POSTGRADUATE SCHOOL
Monterey, California

THESIS

An Investigation of the Production
of Nitric Oxide by Soft Solar X-Rays
in the E-Region of the Ionosphere

by

Richard Allen Dumas

December 1988

Thesis Advisor: David D. Cleary

REPORT DOCUMENTATION PAGE

1a REPORT SECURITY CLASSIFICATION UNCLASSIFIED		1b RESTRICTIVE MARKINGS		
2a. SECURITY CLASSIFICATION AUTHORITY		3. DISTRIBUTION/AVAILABILITY OF REPORT Approved for public release; distribution is unlimited.		
2b DECLASSIFICATION/DOWNGRADING SCHEDULE				
4 PERFORMING ORGANIZATION REPORT NUMBER(S)		5 MONITORING ORGANIZATION REPORT NUMBER(S)		
6a NAME OF PERFORMING ORGANIZATION Naval Postgraduate School	6b OFFICE SYMBOL (If applicable) 33	7a. NAME OF MONITORING ORGANIZATION Naval Postgraduate School		
6c. ADDRESS (City, State, and ZIP Code) Monterey, CA 93943-5000		7b. ADDRESS (City, State, and ZIP Code) Monterey, CA 93943-5000		
8a. NAME OF FUNDING/SPONSORING ORGANIZATION	8b OFFICE SYMBOL (If applicable)	9. PROCUREMENT INSTRUMENT IDENTIFICATION NUMBER		
8c. ADDRESS (City, State, and ZIP Code)		10. SOURCE OF FUNDING NUMBERS		

10. SOURCE OF FUNDING NUMBERS			
PROGRAM ELEMENT NO.	PROJECT NO	TASK NO	WORK UNIT ACCESSION NO

11. TITLE (Include Security Classification)

AN INVESTIGATION OF THE PRODUCTION OF NITRIC OXIDE BY SOFT SOLAR X-RAYS IN THE E-REGION OF THE IONOSPHERE

12 PERSONAL AUTHOR(S) Dumas, Richard, A.

13a TYPE OF REPORT Master's Thesis	13b TIME COVERED FROM _____ TO _____	14. DATE OF REPORT (Year, Month, Day) December 1988	15 PAGE COUNT 65

16 SUPPLEMENTARY NOTATION The views expressed in this thesis are those of the author and do not reflect the official policy or position of the Department of Defense or the U.S. Government

17	COSATI CODES		18. SUBJECT TERMS (Continue on reverse if necessary and identify by block number)
FIELD	GROUP	SUB-GROUP	Photochemical Model; Nitric Oxide Solar X-rays; Thermosphere.

19 ABSTRACT (Continue on reverse if necessary and identify by block number)

The production of nitric oxide by soft solar X-rays in the E-region of the ionosphere is investigated. An empirical expression for the variation in X-ray flux as a function of F10.7 is determined. This expression is incorporated into a one dimensional diffusive photochemical model to compute nitric oxide densities. The results of these calculations are compared with NO observations from the Solar Mesosphere Explorer satellite. Variations of X-ray flux by a factor of 30 over the solar cycle can explain the observed variation in nitric oxide densities.

20 DISTRIBUTION/AVAILABILITY OF ABSTRACT ☐ UNCLASSIFIED/UNLIMITED ☒ SAME AS RPT ☐ DTIC USERS	21. ABSTRACT SECURITY CLASSIFICATION Unclassified	
22a NAME OF RESPONSIBLE INDIVIDUAL David D. Cleary	22b TELEPHONE (Include Area Code) (408) 646-2828	22c OFFICE SYMBOL 61-C1

DD FORM 1473, 84 MAR

83 APR edition may be used until exhausted
All other editions are obsolete

SECURITY CLASSIFICATION OF THIS PAGE

☆ U.S. Government Printing Office: 1986—606 243

UNCLASSIFIED

An Investigation of the Production
of Nitric Oxide by Soft Solar X-Rays
in the E-Region of the Ionosphere

by

Richard Allen Dumas
Lieutenant, United States Navy
B.S., University of Utah, 1982

Submitted in partial fulfillment of the
requirements for the degree of

MASTER OF SCIENCE IN PHYSICS
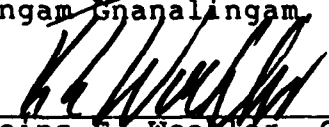
from the

NAVAL POSTGRADUATE SCHOOL
December, 1988

Author: _____
Richard A. Dumas

Approved By: _____
David D. Cleary, Thesis Advisor

_____
Suntharalingam Gnanalingam, Second Reader

_____
Karlheinz E. Woehler, Chairman,
Department of Physics

_____
Gordon E. Schacher
Dean of Science and Engineering

ABSTRACT

The production of nitric oxide by soft solar X-rays in the E-region of the ionosphere is investigated. An empirical expression for the variation in X-ray flux as a function of F10.7 is determined. This expression is incorporated into a one dimensional diffusive photochemical model to compute nitric oxide densities. The results of these calculations are compared with NO observations from the Solar Mesosphere Explorer satellite. Variations of X-ray flux by a factor of 30 over the solar cycle can explain the observed variation in nitric oxide densities.

Accession For

NTIS GRA&I	X
DTIC TAB	☐
Unannounced	☐
Justification	

By

Distribution/

Availability Codes

| Dist | Avail and/or Special |
| A-1 | |

DTIC
COPY
INSPECTED
6

TABLE OF CONTENTS

I. INTRODUCTION

This thesis investigates the production of nitric oxide (NO) by solar soft X-rays in the E-region of the ionosphere over the solar cycle. The variation between extreme ultraviolet (EUV) flux and X-ray flux as a function of solar cycle is investigated as the principal factor influencing NO production in the E-region. This research was prompted by the hypothesis of Barth et al. (1988) that nitric oxide variations are produced by variations in the solar soft X-ray flux between 20 and 100 Å. The main topic will be an analysis of the production of nitric oxide at 110 km as measured by the Solar Mesosphere Explorer (SME) satellite. These measurements are compared to the results of a one-dimensional diffusive photochemical model developed by Cleary (1985) at the University of Colorado and modified by Siskind (1988) to allow for large variations in the solar X-ray flux between 18.62 and 50 Å.

A. THESIS GOALS

This thesis is a theoretical and observational study of the production of nitric oxide in the E-region of the ionosphere based on variations between EUV and X-ray flux over solar cycle. An empirical expression relating X-ray and EUV flux is sought in order to better model the production and loss of NO in the lower thermosphere.

1

B. THESIS OUTLINE

The thesis is divided into seven chapters. Chapter II presents background information about the composition and structure of the ionosphere, and describes some techniques for measuring the density profile of various constituents. Atmospheric chemistry is reviewed in Chapter III, with the emphasis on photochemistry. The continuity equation and physical transport mechanisms are discussed, as well as the method used by the model in solving the continuity equation. The chemistry of nitric oxide is focused on in section C, and the concept of X-ray scaling is introduced. Chapter IV discusses photochemical modeling and describes the basic structure and operation of the photochemical model used in this thesis. Chapter V proposes an empirical relationship between the X-ray scaling factor (FRACXR) and 10.7 cm flux over solar cycle, with results of comparisons between model data and SME satellite measurements presented in Chapter VI. Chapter VII summarizes the thesis and presents suggestions for further research.

II. BACKGROUND

Nitric oxide makes up only 0.5 parts per billion of the Earth's total atmosphere (NOAA, 1976), yet its role as a catalyst in the destruction of stratospheric ozone makes it one of the most important trace constituents. The ionization of NO by geocoronal Lyman-α is largely responsible for maintaining the nighttime E-region ionization at about 100 km. Additionally, because nitric oxide is very reactive, it plays an important role in the daytime ionospheric character. Because this thesis concentrates on ionospheric NO production, a brief description of the ionosphere is presented.

A. THE IONOSPHERE

Above about 60 km, there are sufficient ions and electrons to create a region which affects the propagation of radiowaves. This region is called the ionosphere. The ionosphere is neutral overall. It is composed mostly of neutral molecular and atomic gasses which have concentrations that are several orders of magnitude greater than the ions and electrons. The variation of electron density with altitude leads to three natural subdivisions within the ionosphere. These three regions are called the D, E, and F regions. The F-region is further divided into two subregions called the F1- and F2-regions. This character-

istic "layering" of the ionosphere is due to the variation
of atmospheric composition with altitude and the wide range
of ionizing wavelengths associated with each neutral
species.   Figure 2.1 shows the different regions of the
ionosphere.
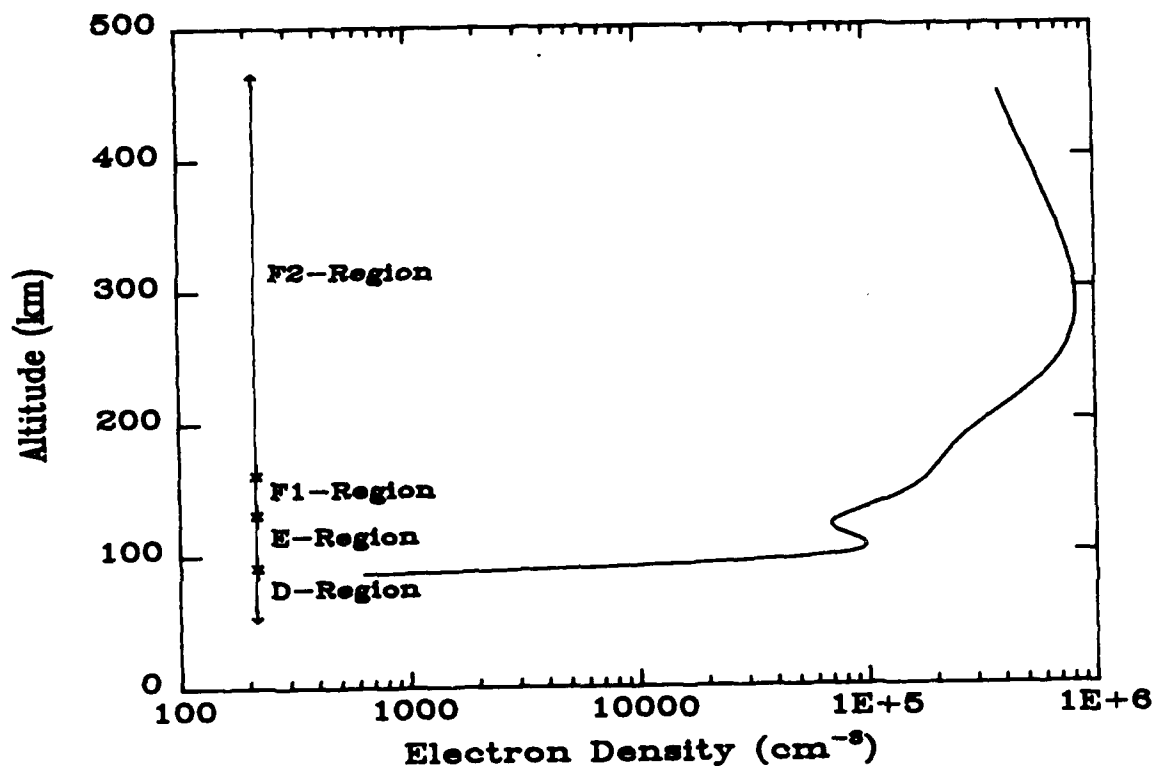
Figure 2.1.   Regions of the Ionosphere.

1. The D-Region

The D-region is the lowest lying ionospheric region and is therefore produced by ionizing radiation at those frequencies which penetrate deepest into the atmosphere. It extends from about 50 to 90 km in altitude. The major source of ionization in the D-region is photoionization of NO by the Lyman-α 1215.7 Å line.

2. The E-Region

The E-region lies between about 90 and 130 km, and has a daytime electron density about two orders of magnitude greater than that of the D-region. Ionization in this region is primarily due to photoionization of molecular oxygen and nitrogen by EUV and soft X-rays.

3. The F-Region

In the F-region, above 130 km, O, O_2, and N_2 all photoionize, with the primary source above 150 km being atomic oxygen. Within the region, the electron density is fairly uniform until about 160 km, where it then rises to a daytime maximum of approximately $10^6/cm^3$ at 220-450 km. Because of this characteristic profile, the F-region is further divided into the F1- and F2-regions lying at 130-160 km and 160-600 km respectively. In the F1-region, ion chemistry dominates the characterization of the ionosphere whereas in the F2-region physical transport (i.e., diffusion) is the most important process.

B. THE THERMOSPHERE

The Earth's neutral atmosphere is divided into regions primarily on the basis of temperature gradients. Typically, at middle latitudes, the temperature falls with increasing altitude until reaching a local minimum of around 200 K at about 10 km. Here the atmosphere undergoes a temperature inversion where the temperature rises with increasing altitude until a local maximum of 290 K is reached at about 50 km. The atmospheric temperature then again falls with increasing altitude until an absolute minimum of about 160 K is reached at 90 km. This minimum is termed the mesopause and marks the beginning of the <u>thermosphere</u>. In the thermosphere, temperature again increases with altitude, approaching a maximum value in the region of 1000-2000 K at a height of several hundred kilometers. Above the thermosphere, the atmosphere is essentially isothermal.

C. REMOTE SENSING TECHNIQUES

Because the ionosphere is a plasma, it will affect the propagation of radio waves. It is for this reason that radio sounding methods were the first experimental techniques used for studying the ionosphere (see e.g., Bauer, 1973). Other techniques can be used to obtain experimental information about the chemistry and chemical processes of the atmosphere. Among the most important of these are ground-based observations of airglow emissions and the use of satellite-borne photometers and spectrometers.

1. **Remote Sensing of Chemical Processes**

    a. Ground-based Airglow Observations

    The term airglow is used to describe non-auroral light emissions from the upper atmosphere. These emissions are extremely weak and therefore require very sensitive equipment to be detected. A common instrument used for airglow measurements is the scanning monochromator which detects light in a very narrow bandwidth. A major difficulty encountered in airglow detection is the isolation of the emission from the strong background of scattered sunlight. (see e.g., McEwan and Phillips, 1975)

    b. Satellite Observations

    Satellite airglow observations offer an advantage over ground observations in that there is almost no scattered sunlight to obscure the actual airglow emissions. An additional advantage lies in the geometry of satellite limb viewing (see e.g., Liou, 1980). This makes possible the calculation of the column density of an emitting species. Through an "onion-skin" inversion method the number density of the emitting species can then be calculated (see e.g., Cleary, 1985; Hickman et al., 1977).

2. **Radio Sounding of the Ionosphere**

    Electron density profiles of the ionosphere can be measured using a variable frequency radar which measures the time delay between the transmission of an RF pulse and its

echo from a reflecting level within the ionosphere (see
e.g., Bauer, 1973). Such a device is called an _ionosonde_.

The requirement for reflection of an electromagnetic
wave from an ionized medium is that the magnitude of the
complex propagation vector, κ, be imaginary. This require-
ment is met when

$$\frac{[e]e^2}{\varepsilon_0 m\omega^2} > 1. \qquad (2.1)$$

The value of ω for which equation (2.1) is identically one
is ω_p, the plasma frequency. The index of refraction, n, in
the ionized medium is given by

$$n = \left(1 - \frac{\omega_p^2}{\omega^2}\right)^{\frac{1}{2}} = \left(1 - \frac{80.6[e]}{f^2}\right)^{\frac{1}{2}}. \qquad (2.2)$$

The requirement for reflection of an electromagnetic wave at
normal incidence is n = 0. Thus the maximum frequency for
normal reflection is given by

$$f^2 = 80.6[e] \qquad (2.3)$$

where f is measured in Hz and [e] is the electron density in
electrons/m^3. Thus by varying the frequency it is possible
to map out the electron density profile. However,
examination of Figure 2.1 shows that the electron density
above about 250 km cannot be measured by ground-based

8

ionosondes because the frequencies needed to probe this region will already have been reflected at a lower altitude.

In order to obtain electron density profiles for the region above 250 km, ionosondes have been placed on satellites. Top-side sounding is a very valuable technique for obtaining electron density profiles in the upper F2-region. Unfortunately, most of the measurements taken from top-side ionosondes do not provide full profiles down to the peak altitude so that it is difficult to merge this data with that of ground-based ionosondes.

III. CHEMICAL REACTIONS IN THE THERMOSPHERE

A great variety of atoms and molecules exist in the thermosphere. As will be discussed later, much of this molecular soup is subject to reaction with solar radiation. The resulting photolytically generated species undergo many different chemical processes with the surrounding atmosphere. This chapter will examine these processes and introduce the method used for analyzing the rapidly changing composition and structure of the thermosphere.

A. PRINCIPLES OF PHOTOCHEMISTRY

Photochemistry is concerned with chemical reactions that are initiated by the absorption of solar radiation. The absorption process is written as

$$A + h\nu \rightarrow A^*, \tag{3.1}$$

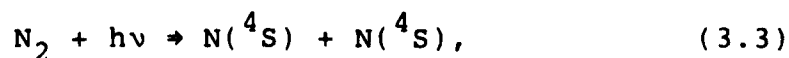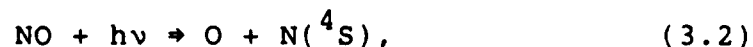where A^* is an excited energy state of molecule A. The excited state could be a rotational or vibrational level, an electronic state, or it could represent the decomposition of the molecule into two or more fragments. This latter process is called photodissociation or photolysis if the products are all neutral atoms or molecules, and is called photoionization if the products include an ion and one or more electrons.

Once excited molecules or atoms are produced, they undergo secondary chemical reactions, forming species that would not exist in a normal state of local thermal equilibrium (LTE). Therefore these photochemical processes are non-LTE mechanisms and must be quantitatively analyzed by studying the rate at which reaction occurs (see e.g., Chamberlain,1978).

1. Photodissociation

The process by which the absorption of a photon leads to disruption of the absorbing molecule is called photodissociation or photolysis. The atoms produced in this manner are highly reactive. Photolysis processes which take place in the photochemical model used for this thesis are:

$$NO + h\nu \rightarrow O + N(^4S), \qquad (3.2)$$

$$N_2 + h\nu \rightarrow N(^4S) + N(^4S), \qquad (3.3)$$

and

$$N_2 + h\nu \rightarrow N(^2D) + N(^2D). \qquad (3.4)$$
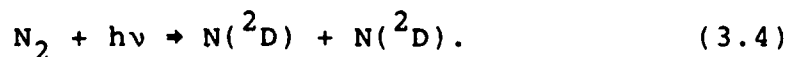
Notice that the last two equations involve the photodissociation of molecular nitrogen into two different electronic states of elemental nitrogen. The extent to which these two reactions occur is given by their branching ratios. For the above two reactions, the branching ratio for each has been determined to be 0.5, indicating that half

11

of the reactions which occur will produce $N(^4S)$ and that the other half will result in $N(^2D)$ production (see e.g., Heiklen, 1976).

a. Photodissociation Rates

There are three factors influencing the rate of photodissociation : molecular concentration, photon flux, and quantum yield. The most obvious factor must be the amount, or concentration, of molecule A. Concentrations of a substance per unit volume are denoted by enclosing the substance in square brackets. [A] is the concentration of substance A per unit volume.

Another factor influencing the rate is the number of photons available to cause photodissociation. The flux of solar radiation outside the atmosphere is simply a function of the brightness of the Sun and the distance from the Sun. However, as the radiation penetrates the Earth's atmosphere the flux of photons is attenuated due to absorption by atmospheric gasses. At high altitudes the atmospheric density is low and therefore little absorption takes place. As the altitude decreases the density increases, and absorption becomes important.

The efficiency, or quantum yield of the reaction given by equation (3.1) is defined as the number of A^* molecules produced for each absorbed photon. Quantum yield varies with wavelength and is zero longward of the ionization wavelength.

12

A common way of expressing the photon flux at a particular altitude z is in terms of the exoatmospheric flux and the _optical depth_. Optical depth, τ, is defined as

$$\tau = \sum_i \sigma_a(i) \int_z^\infty [i] dz',$$
(3.5)

where σ_a is the absorption cross section for the ith constituent at a specific wavelength, and [i] is the concentration of that constituent. The photon flux is then given by

$$\Phi(z) = \Phi_\infty e^{-\tau \cdot \sec(\chi)},$$
(3.6)

where $\Phi(z)$ is the photon flux at altitude z, Φ_∞ is the exo-atmospheric photon flux, τ is optical depth, and χ is the solar zenith angle. Note that $\tau \cdot \sec(\chi)$ is the optical pathlength through the atmosphere.

2. Photoionization

When the products of equation (3.1) include molecular or atomic ions and one or more electrons, the process is called photoionization. Schematically this is written

$$A + h\nu \rightarrow A^+ + e^*.$$
(3.7)

In this process, the energy carried in by the photon is converted into ionization energy plus kinetic energy of the electron. These energetic electrons are called _photo-_

13

electrons, (e^*), and enter into several different energy transfer reactions with neutral gasses.

The major source of ionizing radiation in the thermosphere is solar radiation. The only wavelengths which penetrate to the E-layer are extreme ultraviolet (EUV), X-rays, and Lyman-α.

a. Photoionization Rates

The rate at which photoionization takes place for each constituent is described by its <u>ionization rate</u>. For a given constituent, the ionization rate is given by

$$q_i(z) = \int \sigma_i(\lambda) \cdot \Phi_z(\lambda) \, d\lambda, \qquad (3.8)$$

where σ is the ionization cross section and Φ_z is the solar flux at altitude z. (Torr et al., 1979)

B. DIFFUSION AND THE CONTINUITY EQUATION

It is possible to construct an equation showing the time variation of a particular constituent's concentration once the rate coefficients for the production and loss mechanisms are known. This equation is called the <u>continuity equation</u> and contains terms relating the chemical creation and destruction of the constituent, as well as terms describing the flux due to physical transport processes. There are four types of physical transport mechanisms: <u>molecular diffusion</u>, <u>ambipolar diffusion</u>, <u>eddy diffusion</u>, and <u>thermal diffusion</u>.

1. Molecular and Ambipolar Diffusion

When the concentration gradient of a constituent in the atmosphere differs from its equilibrium value, the resulting motion is called molecular diffusion. For an isothermal atmosphere, this can be written

$$\Phi_i = -D_i \left(\frac{\partial [i]}{\partial z} + \frac{[i]}{H_i} \right) \qquad (3.9)$$

where Φ_i is the flux, D_i is the molecular diffusion coefficient, and H_i is the scale height for the ith constituent.

Diffusion which results from a concentration gradient of a charged constituent in a partially ionized gas, or plasma, in which the constituent is influenced by the electrostatic forces of the plasma as a whole is called ambipolar diffusion. Although electrons in the thermosphere have a greater diffusion coefficient than the ions, electrostatic attraction between electrons and positive ions prevents any large scale separation. Thus the plasma diffuses as a whole, with ambipolar diffusion coefficient D_a. (see e.g., McEwan and Phillips, 1975)

2. Eddy Diffusion

Eddy diffusion is the result of turbulent mixing in the presence of a composition gradient. Whereas molecular diffusion results from the average velocity of the constituent being different from that of others, eddy diffusion occurs whether or not there is any difference in

15

average molecular velocity between the constituents. Eddy diffusion can be expressed similarly to molecular diffusion by an equation analogous to (3.8). The coefficient of molecular diffusion D_i is replaced by the eddy diffusion coefficient K.

3. Thermal Diffusion

Thermal diffusion is due to large temperature gradients in a gas mixture. It can be properly accounted for only in a rather complex manner. However, since the thermal diffusion factor α_i is proportional to the difference in molecular weights of the constituent gasses, thermal diffusion is important in the atmosphere only for light gasses such as hydrogen and helium. Because the model used in this thesis is primarily concerned with the chemistry of nitric oxide, thermal diffusion can be neglected.

4. The Continuity Equation

Physical transport and chemical processes act on each constituent of the atmosphere to produce a variation in concentration with time. The equation which governs these processes is the mass continuity equation

$$\frac{\partial[i]}{\partial t} + \frac{\partial}{\partial z}\Big([i]\cdot v_i\Big) = P_i - L_i[i]. \qquad (3.10)$$

16

Again, [i] is the concentration at time t and altitude z, P_i and $L_i[i]$ are chemical production and loss rates, and V_i is the mean vertical velocity due to transport processes. Since $[i] \cdot V_i$ is the vertical flux Φ_i, the second term in equation (3.9) may be written

$$\frac{\partial}{\partial z}\left([i] \cdot V_i\right) = \frac{\partial \Phi_i}{\partial z}. \qquad (3.11)$$

For a neutral constituent with low concentration, Φ_i may be written as the sum of molecular and eddy diffusion. Thus

$$\Phi_i = -D_i \left(\frac{\partial[i]}{\partial z} + \frac{[i]}{T}\frac{\partial T}{\partial z} + \frac{[i]}{H_i}\right) - K \left(\frac{\partial[i]}{\partial z} + \frac{[i]}{T}\frac{\partial T}{\partial z} + \frac{[i]}{H_{av}}\right),$$

$$(3.12)$$

where the middle terms are due to the dependence of scale height on temperature gradient, D_i and K are the molecular and eddy diffusion coefficients respectively, T is the absolute temperature, H_i the scale height for the ith constituent, and H_{av} the scale height for a constituent having the mean molecular mass. (Colgrove et al., 1966)

a. Time Constants

The continuity equation includes chemical and dynamical processes. The dominance of one process over another can be determined by examining the relative magnitude of the characteristic times, or time constants, of the competing processes (Goody and Walker, 1972). If two processes are competing and one acts more rapidly than the

17

other, the faster one will be more effective. The dominant process will be the one with the shorter time constant (see e.g., Wallace and Hobbs, 1977).

By performing dimensional analysis on the continuity equation, the time constants for chemistry, τ_C, eddy diffusion, τ_K, and molecular diffusion, τ_D, can be approximated (Cleary, 1985). The distribution of [i] is determined principally by chemistry if $\tau_C < \tau_K$ and $\tau_C < \tau_D$, and by dynamics if $\tau_K < \tau_C$ and $\tau_D < \tau_C$.

A comparison of the lifetimes for molecular diffusion, eddy diffusion, and chemical destruction was done by Cleary (1985) for the different species used in that model. The comparison showed that dynamical processes are only important for two species, NO and $N(^4S)$. For the remaining species $(N(^2D),\ NO^+,\ O_2^+,\ N_2^+,\ O^+,\ and\ O(^2D)^+)$, chemical processes are sufficiently fast that transport may be neglected (Cleary, 1985). Ambipolar diffusion for O^+ was later added to the model.

5. Solutions to the Continuity Equation

For constituents which have sufficiently short chemical time constants, the dynamical processes of diffusion may be neglected. Thus the flux term in equation (3.10) vanishes and the continuity equation reduces to

$$\frac{\partial [i]}{\partial t} = P - L[i] \qquad (3.10a)$$

for $N(^2D),\ NO^+,\ O_2^+,\ N_2^+,\ O^+,\ and\ O(^2D)^+$.

18

For those constituents which have short dynamical time constants (i.e., NO and $N(^4S)$), the flux term in the continuity equation must be retained. When the expression for ϕ given by equation (3.12) is substituted into equation (3.10) and differentiated, a parabolic differential equation results. This equation can be written

$$\frac{\partial [i]}{\partial t} = A_i \frac{\partial^2 [i]}{\partial z^2} + B_i \frac{\partial [i]}{\partial z} + C_i [i] + E_i. \qquad (3.13)$$

The coefficients A_i, B_i, C_i, and E_i in equation (3.13) are given in Table I. Equations (3.10a) and (3.13) cannot be solved analytically and must be solved by numerical methods. In the model used for this thesis, the method is the Crank-Nicolson finite differencing technique. (Cleary, 1985 App. A)

C. CHEMICAL REACTIONS IN THE LOWER THERMOSPHERE

Many types of chemical reactions are continually taking place in the atmosphere. Products of these reactions include photolytically generated atoms, radicals, excited molecules and ions. As was seen in previous sections, photoionization and photodissociation are the primary photochemical reactions. Reactions involving the products of these two types of reactions with themselves and with the stable atmospheric gasses determine in great part the characteristics of the atmosphere.

```
┌─────────────────────────────────────────────────────────────┐
│                         TABLE I                               │
│                                                               │
│     COEFFICIENTS TO THE PARABOLIC DIFFERENTIAL EQUATION       │
├─────────────────────────────────────────────────────────────┤
```

$$A_i = D_i + K$$

$$B_i = \left(\frac{\partial D_i}{\partial z} + \frac{\partial K}{\partial z}\right) + \left(\frac{D_i + K}{T}\right)\frac{\partial T}{\partial z} + \left(\frac{D_i}{H_i} + \frac{K}{H}\right)$$

$$C_i = \left(\frac{\partial D_i}{\partial z} + \frac{\partial K}{\partial z}\right)\frac{1}{T}\frac{\partial T}{\partial z} - \left(\frac{D_i + K}{T^2}\right)\left(\frac{\partial T}{\partial z}\right)^2$$

$$+ \left(\frac{D_i + K}{T}\right)\frac{\partial^2 T}{\partial z^2} + \frac{1}{H_i}\frac{\partial D_i}{\partial z} + \frac{D_i}{(H_i)^2}\frac{\partial H_i}{\partial z}$$

$$+ \frac{1}{H}\frac{\partial K}{\partial z} - \frac{K}{H^2}\frac{\partial H}{\partial z} - L_i$$

$$E_i = P_i$$

```
└─────────────────────────────────────────────────────────────┘
```

The appendix summaries the types of chemical processes which are important in the execution of the one dimensional model used in this thesis for the calculation of nitric oxide in the thermosphere. Of course, many other reactions also occur, but it is the chemistry of nitric oxide which is germane to this investigation.

1. Nitric Oxide Chemistry

Direct sources of nitric oxide in the E-region are the reactions of atomic nitrogen (ground state $N(^4S)$ and excited states $N(^2D)$ and $N(^2P)$) with molecular oxygen. These three reactions (R28, R29, and R39 of Appendix) do not equally contribute to the production of NO. In steady state, the NO production rate of each reaction is found by multiplying the rate coefficient by the product of the concentrations of the reactants. Figure 3.1 shows some typical daytime nitrogen density profiles. Figure 3.2 shows the corresponding NO production rates from the three different atomic nitrogen states, as well as the rate coefficient (k) for each reaction. It can be seen from Figure 3.2 that the principal source of NO at 110 km is $N(^2D)$ via the reaction

$$N(^2D) + O_2 \rightarrow NO + O \qquad (3.14)$$
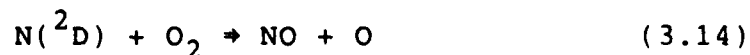
The small contribution from $N(^4S)$ is due to the temperature dependence of the rate coefficient, and the small contribution from $N(^2P)$ is because of its low concentration.

Sources of $N(^2D)$ are from the dissociative recombination of N_2^+ and NO^+ (R19 and R27), the dissociative excitation by photoelectrons of N_2 (R12), the photo-dissociation of N_2 (R15), and the ion-atom interchange between N_2^+ and O (R17). In a method analogous to that used for NO production, it can be shown that the two principal

21
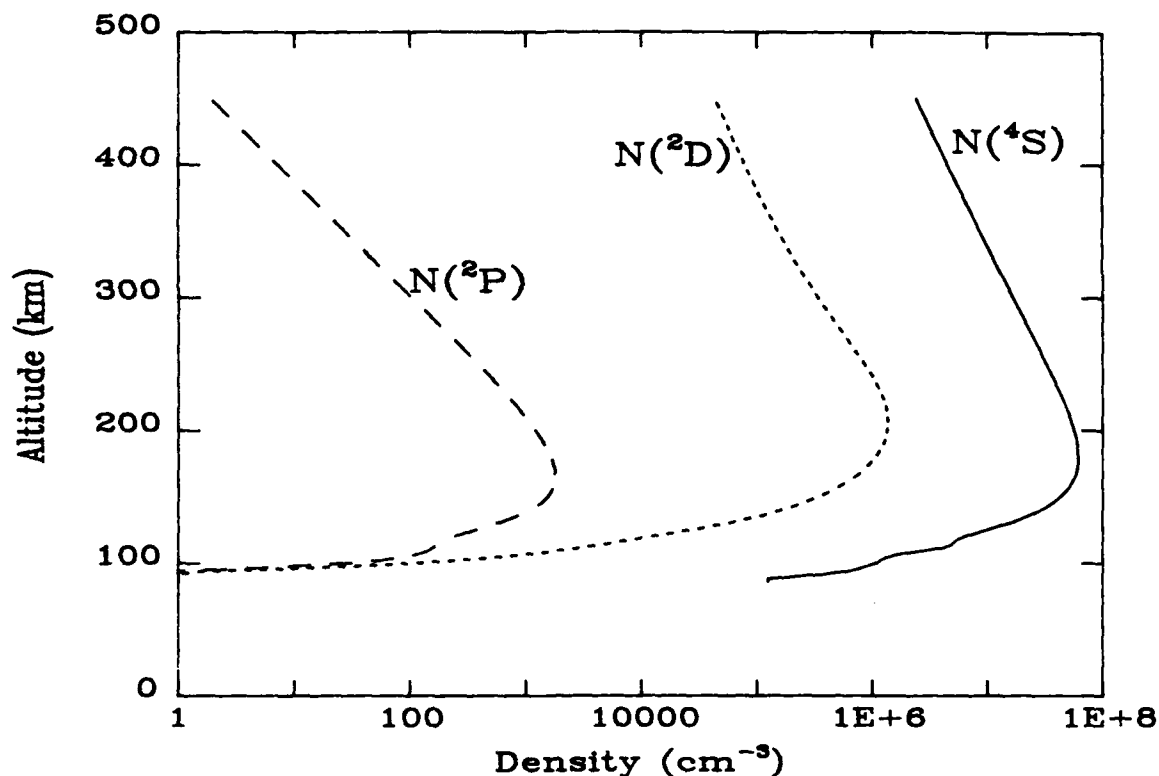
Figure 3.1. Atomic Nitrogen Densities.

sources of $N(^2D)$ are via R27 and R12. These equations are stated here for ease of reference

$$NO^+ + e \rightarrow O + N(^2D) \qquad\qquad R27$$

$$N_2^+ + e^* \rightarrow N(^2D) + N(^2D) + e \qquad\qquad R12$$
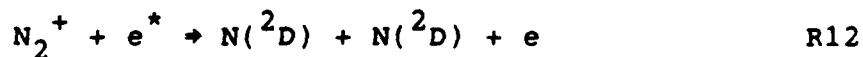
The two loss processes for nitric oxide in the E-region are via the bimolecular reaction with $N(^4S)$, (R33), and the charge exchange with O_2^+, (R22)

$$N(^4S) + NO \rightarrow N_2 + O \qquad\qquad R33$$

$$O_2^+ + NO \rightarrow NO^+ + O_2 \qquad\qquad R22$$
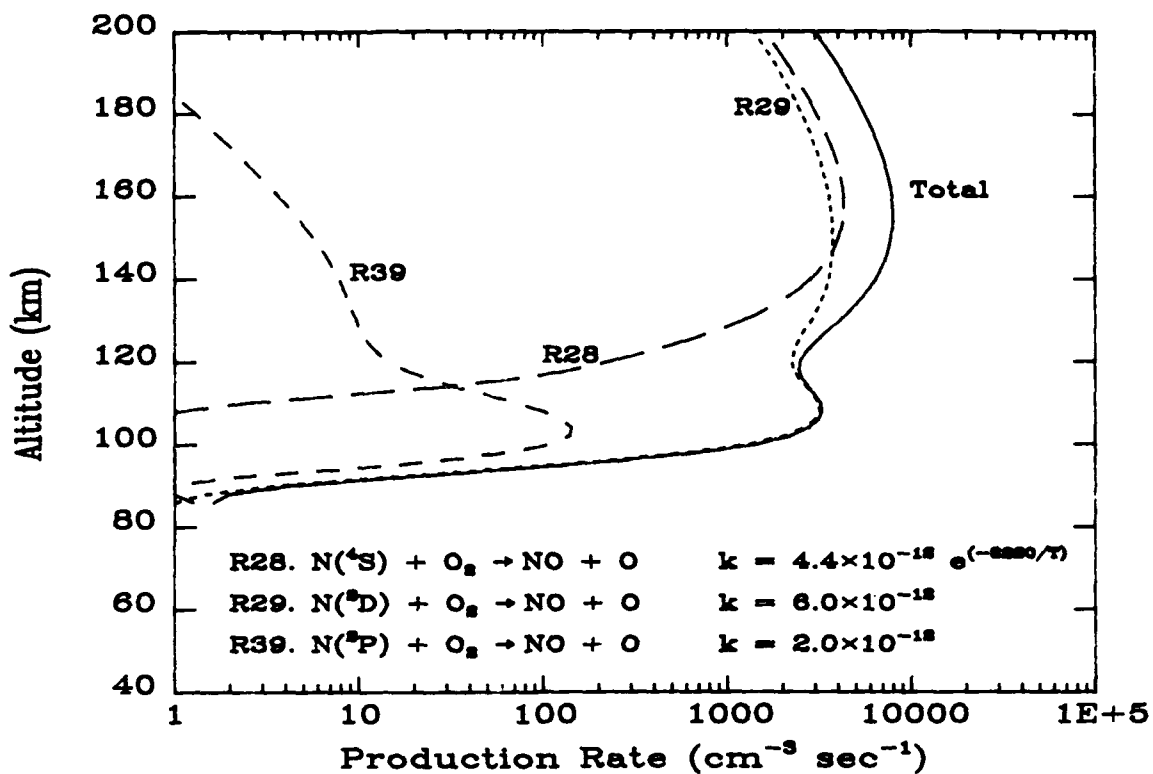
Figure 3.2. NO Production Rates

In the figure, legend reactions:

R28. $N(^4S) + O_2 \rightarrow NO + O$ $k = 4.4 \times 10^{-12} e^{(-3220/T)}$

R29. $N(^2D) + O_2 \rightarrow NO + O$ $k = 6.0 \times 10^{-12}$

R39. $N(^2P) + O_2 \rightarrow NO + O$ $k = 2.0 \times 10^{-12}$

Thus, while $N(^2D)$ is a source of nitric oxide at 100 km, $N(^4S)$ is both a source and sink. An analysis of these production and loss processes as they pertain to the photochemical model is presented in Chapter V.

IV. THE PHOTOCHEMICAL MODEL

A. PHOTOCHEMICAL MODELING

Photochemical modeling is a useful tool for gaining an understanding of the minor constituents in the thermosphere. By comparing a theoretical model with observations of some constituents for which data are available, one can determine the validity of the model and better understand physical and chemical mechanisms occurring in the thermosphere.

"Photochemical models are sensitive to various input parameters such as solar fluxes, photoabsorption cross-sections, chemical reaction schemes and reaction rate constants, and transport parameters (e.g., eddy diffusion coefficient) as well as to the method of numerical analysis and boundary conditions." (Shimazaki, 1985). Additionally, models may be time dependent or time independent. Time independent models are usually used to arrive at a steady-state condition. A steady-state model does not represent the actual state for the constituents whose concentrations change as a function of time. Causes for these changes would be solar flux, geomagnetic Ap index, and any temperature dependent reaction rate since the temperature is also time dependent. Time dependent models attempt to account for these temporal variations.

24

B. THE TIME DEPENDENT PHOTOCHEMICAL MODEL

1. Numerical Technique

In Chapter III it was shown that the three phenomena which must be understood in order to model an atmospheric constituent properly are chemistry, eddy diffusion, and molecular diffusion. Additionally, it was shown that the continuity equation reduces to equation (3.10a) for species which do not require transport processes to be considered. For NO and $N(^4S)$ transport processes must be included and the continuity equation becomes a parabolic differential equation (equation (3.13)).

Equation (3.10a) can be solved by the following semi-implicit finite difference equation

$$\frac{([i]_{t+1} - [i]_t)}{\Delta t} = P_t - L_t[i]_{t+1} , \qquad (4.1)$$

which is solved for $[i]_{t+1}$, where $[i]_{t+1}$ is the density of the ith constituent at time interval t+1 and is a function of $[i]_t$.

Equation (3.13) is first order in the time derivative and second order in the spatial derivative and therefore requires three boundary conditions: one in time and two in space. Cleary (1985) has shown and Siskind (1988) has verified that the spatial boundary conditions are satisfied by specifying conditions at the upper and lower altitude limits of the model. Several different spatial

conditions can be used to implement these boundary conditions. The ones used by the model require that there be zero flux of both NO and $N(^4S)$ at the upper boundary, and at the lower boundary the condition for NO is that there is a local minimum in the density profile, while for $N(^4S)$ the requirement is that it be in a state of photochemical equilibrium.

When equation (3.13) is cast into its finite difference form using the Crank-Nicolson method, a series of coupled algebraic equations are produced which can be expressed as a tri-diagonal matrix equation. The density profile for each time increment is obtained using the Thomas algorithm of matrix inversion. (Von Rosenberg, 1969; Cleary, 1985)

2. Inputs to the Model

The Cleary time dependent photochemical model is run in three distinct steps. The first step uses the MSIS-83 program (Hedin, 1983) to calculate the neutral atmosphere. The second step uses a modification of the NRL photoelectron code PEGFAC (NRL Memorandum Report 5004, 1982) to calculate photoelectron impact rates. Siskind (1988) modified the PEGFAC code to extend the energy grid so as to include soft X-rays up to 666 eV (18.62 Å). The existing energy grid was also updated to reflect more recent data. The third step is the actual one dimensional model. The model calculates the

time development of each species which enters into the chemistry of nitric oxide.

a. Neutral Atmosphere

The first step of the photochemical model uses the MSIS-83 (Hedin, 1983) code to calculate the neutral atmosphere for each model "hour" of every day for which the model is run. Results are stored as 183 element column vectors. Each "hour" five of these vectors are generated. The first contains information on the geophysical parameters used. These are (1) the exoatmospheric temperature, (2) solar zenith angle, (3) the F10.7 value for the previous day, (4) the 90 day average F10.7 value, (5) geomagnetic Ap index, (6) latitude, (7) longitude, and (8) the X-ray scaling factor, FRACXR. The second vector contains the temperature profile for altitudes from 86 to 450 km in 2 km increments (hence 183 elements). The third fourth and fifth column vectors contain the density profiles of O, O_2, and N_2, respectively. Thus each "hour" is a 183 × 5 array. Each day produces 24 such arrays.

b. Photoelectron Impact Rates

The calculation of photoelectron impact rates was done using the computer program PEGFAC (NRL Memorandum Report 5004, 1982). Recently, Siskind (1988) revised the PEGFAC code to account more properly for the higher energy photoelectrons produced by soft X-rays. He expanded the original 37 EUV intervals from 50-1050 Å (Torr et al., 1979)

27

to include an additional 20 intervals which cover the soft X-ray flux from 18-50 Å. The fluxes used were measured in one of Hinteregger's rockets and are available from the National Space Science Center in a file labelled SC#21REFW (Siskind, 1988).

EUV fluxes are calculated by performing a linear interpolation between the appropriate solar flux periods reported by Torr et al. (1979) based on the value of F10.7 ($\times 10^{-22}$ W m^{-2} Hz^{-1}). Thus the EUV flux is scaled according to F10.7. Since only one measurement of X-ray flux is available, interpolation is not possible. However, in order to explain the observed solar cycle variations of NO, Barth et al. (1988) suggested that the soft X-ray flux exhibits a larger variation with solar activity than EUV. For this reason, Siskind added a multiplicative X-ray flux scaling factor, FRACXR, to the PEGFAC code. The X-ray fluxes used by the model are scaled by the multiplicative factor FRACXR. It is the goal of this thesis to determine the relationship between FRACXR and F10.7.

PEGFAC uses the flux data to calculate the photoionization rates of N_2, O_2, and O, and the photo-dissociation rates of N_2 for each model "hour" of every day for which the model is run. As with MSIS-83, PEGFAC stores the results as 183 element column vectors. For each "hour", four of these vectors are generated. The first three contain the photoionization rates for N_2, O_2, and O,

respectively. The fourth contains the N_2 photodissociation rates. Thus each hour is a 183 × 4 array. Each day produces 24 such arrays.

c. Direct Inputs to the Model

The neutral atmosphere, photoionization rates for N_2, O_2, and O, and the photodissociation rates for N_2 are calculated exterior to the model. The data files created by these two procedures are used as inputs to the model program. The density profiles for the minor species are set to a generic initial condition, and the model is allowed to run in a time independent mode for a sufficient length of time to allow this initial minor atmosphere to reach the steady state conditions which correspond to the starting date of the run. The model "solves" the continuity equation for each of the species involved in the nitric oxide chemistry every 15 minutes using the numerical methods previously described. When the sun is within 15 degrees of the horizon the atmosphere is rapidly changing, therefore the time increment of the model switches to five minutes. As with MSIS-83 and PEGFAC, the model stores the density profile for each minor constituent in a 183 element column vector.

3. Outputs From the Model

The program is written to calculate the density profile for the minor species at 15 minute intervals, or at five minute intervals if the sun is within 15 degrees of the

29

horizon. For the purpose of this thesis, the output has been structured to extract the nitric oxide density at 110 km for each day at 1500 local time. This is because the SME satellite data was taken at an altitude of 110 km at 1500 local time each day. The output is stored in a vector containing N elements, where N is the number of days for which the model was run.

V. ANALYSIS

Chapters III and IV introduced the theory and modeling technique that is used in this thesis. This chapter will present the experimental approach used to determine the relationship between FRACXR and F10.7.

A. SME OBSERVATIONS

Data from the Solar Mesosphere Explorer satellite was provided by Dr. Charles A. Barth of the Laboratory for Atmospheric and Space Physics, University of Colorado (telephone conversation 17 November, 1988). Equatorial latitude nitric oxide data was used for this thesis. This data is the result of averaging measurements from two satellite orbits between 20° north latitude and 20° south latitude. The first orbit took measurements from $20^{\circ}-60^{\circ}$ east longitude, while the second were between $105^{\circ}-147^{\circ}$ west longitude. All measurements were taken at an altitude of 110 km at 1500 local time. The 110 km nitric oxide density for the period January 6, 1982 to April 19, 1985 is shown in Figure 5.1.

1. Analysis of Original Model

Figure 5.2 shows a comparison between SME data and model calculations prior to the addition of Siskind's FRACXR parameter. It clearly shows that the model was inadequate in predicting both the absolute magnitude and variations in
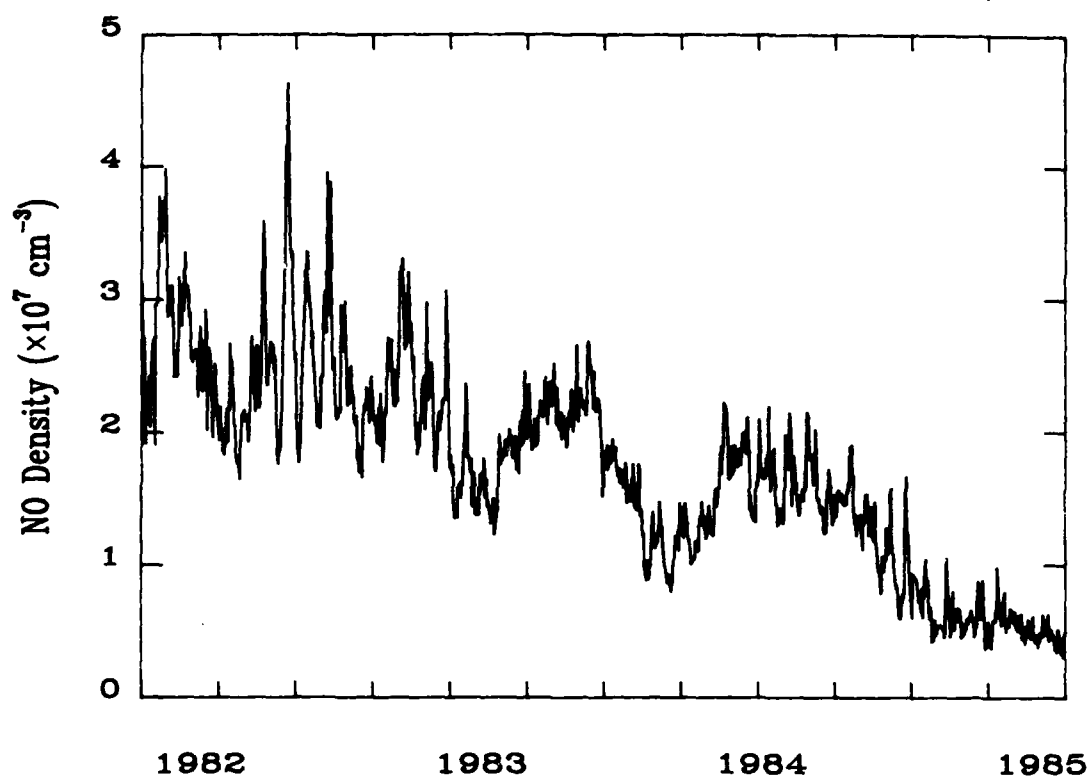
31

Figure 5.1.   Nitric oxide density at 110 km.
SME measurements from January 6,1982 to
April 19, 1985.

the nitric oxide density which were observed by the SME
satellite.   The reason for this inadequacy can be explained
by taking a closer look at the relevant photochemistry.
Originally, an increase in the EUV flux would increase the
rate at which the production of $N(^2D)$ occurs (see R12 and
R27 in Appendix).   However, this increase in EUV flux would
also *cause one of* the principal loss reactions for nitric
oxide (R22) to increase its rate due to an increase in the
ionized molecular oxygen density.   The increase in $N(^2D)$
(and hence NO) was thereby partially offset by the increased
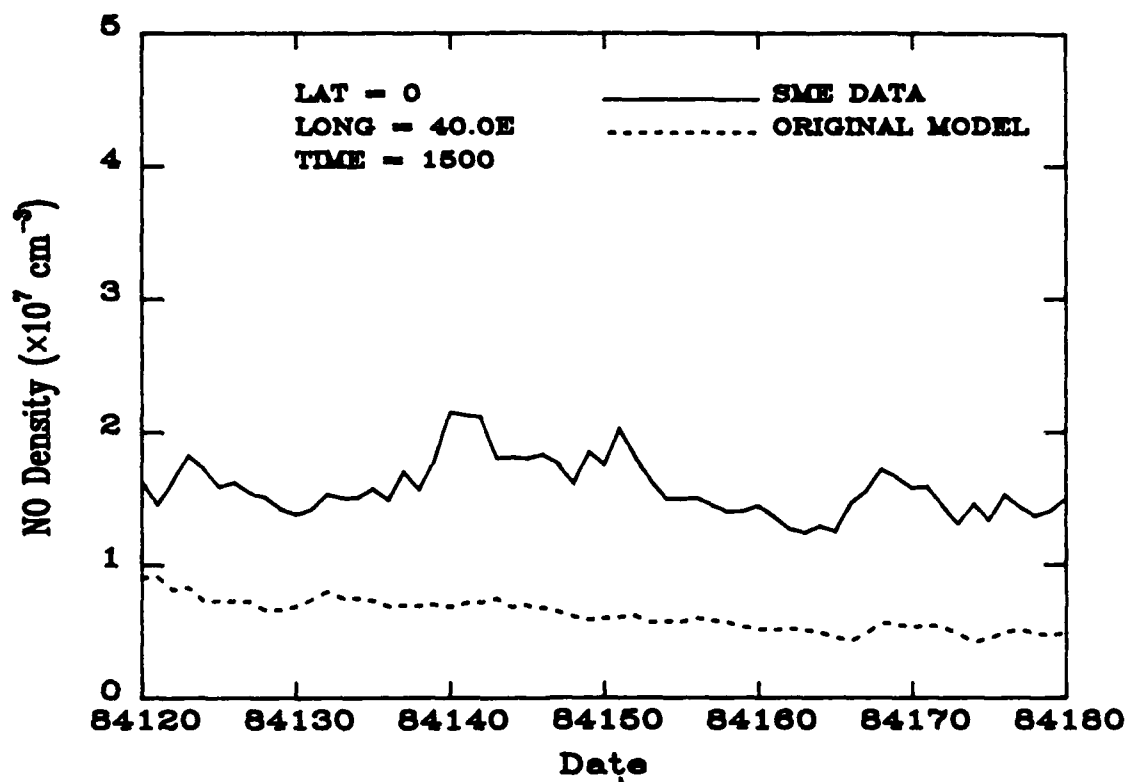loss of NO via R22.   A process was sought which would allow

Figure 5.2. Comparison between SME observations
and the photochemical model prior to FRACXR.

the model to increase the production of $N(^2D)$ without
causing a corresponding decrease in NO density via the
loss reaction R22. This led to the modification of the
PEGFAC code by Siskind as discussed in Chapter IV.

The reason behind the incorporation of the
multiplicative X-ray scaling factor is now clear. Soft
X-rays which penetrate to the E-region photoionize the major
constituents and produce energetic photoelectrons as
discussed in Chapter III. The increase in photoelectrons
drives the production of $N(^2D)$ via R12 and R17, but does not
affect R22. In order for this mechanism to work, the

33

variation in solar X-radiation must be greater than the variation in solar EUV radiation. (Barth et al., 1988)

B. DETERMINATION OF FRACXR

Initial estimates of the magnitude of FRACXR were provided by Siskind (telephone conversation November 9, 1988). He suggested that FRACXR take on values near one for conditions of solar minimum and 50 for solar maximum. This provided a starting point for the determination of the relationship between FRACXR and solar cycle.

1. Assumptions

Two major assumptions were made for the purposes of simplifying the data analysis and reducing computer time. The first assumption is that auroral electrons do not influence the nitric oxide chemistry. This assumption is based on the fact that all computations and observations were at equatorial latitudes. It is justified by the work of Siskind (1988), who showed that for equatorial latitudes there is little enhancement of NO density due to an auroral storm.

The second assumption was that the computation of nitric oxide density would be independent of the longitude at which the model was run. This allowed the model to be run at only one longitude for the computation of each NO density time sequence, instead of averaging two sets of measurements as was done for the SME data. To justify this assumption, the model was run at both 40 degrees east

34

longitude and 126 degrees west longitude for the same five day period in 1982. Figure 5.3 shows the result of this procedure. The two cases deviated from each other by less than 0.2%. Based on this result, all subsequent model runs were done only at 40 degrees east longitude.
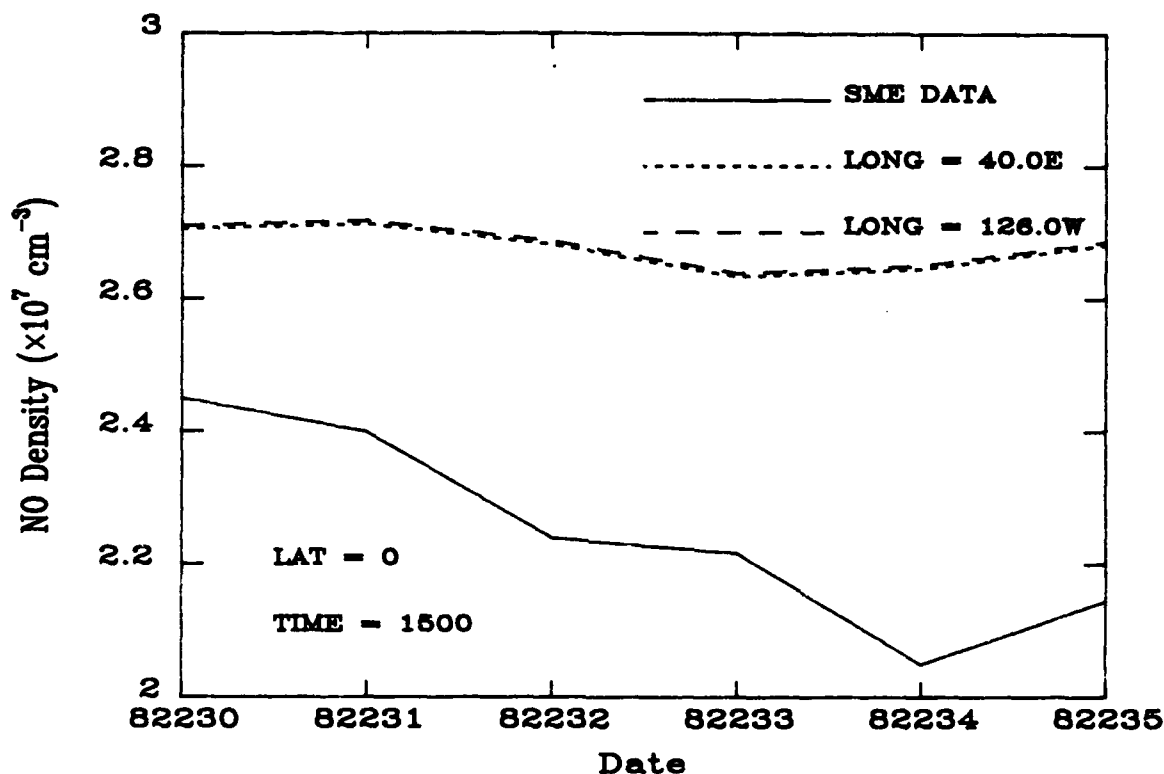

Figure 5.3. Model [NO] calculations for two different longitudes.

2. Experimental Approach

The SME data was searched to locate periods where the value of F10.7 remained constant for at least three days. Four such periods were initially found corresponding to F10.7 ($\times 10^{-22}$ Wm^{-2} Hz^{-1}) values of 70, 90, 128, and 201. The model was then run with various values of FRACXR for

each of the four periods. Figures 5.4 through 5.7 show the results of these runs. This initial data is summarized in Table II and shown graphically in Figure 5.8. Uncertainties are estimated from the data directly without measuring them explicitly since only one set of calculations is possible each time the model is run (see e.g., Bevington,1969).

TABLE II			
SUMMARY OF INITIAL FRACXR DATA			
DATE		F10.7	
START	END	$(\times 10^{-22}\ Wm^{-2}Hz^{-1})$	FRACXR
84300	84303	70	3 ± 2
83297	83300	90	6 ± 1
83185	83188	128	22 ± 2
82169	82171	201	24 ± 1

It can be seen from Figure 5.8 that the first three data points are nearly linear, while the point corresponding to an F10.7 value of 201 lies significantly lower than would be expected using a linear relationship based on the first three points. To resolve this uncertainty, a fifth data point was taken for an F10.7 value of 242. Although this value was constant for only two days, the FRACXR value at this point would determine if a linear relationship was probable. The result of this run is shown in Figure 5.9.
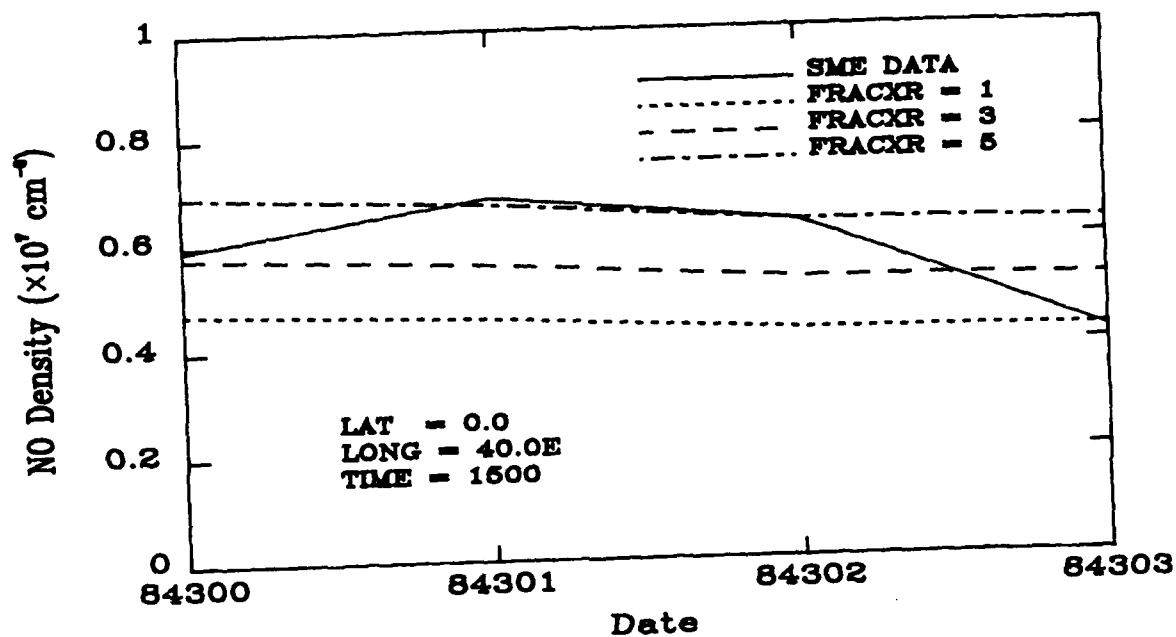
36

Figure 5.4. Model [NO] densities for F10.7 = 70.
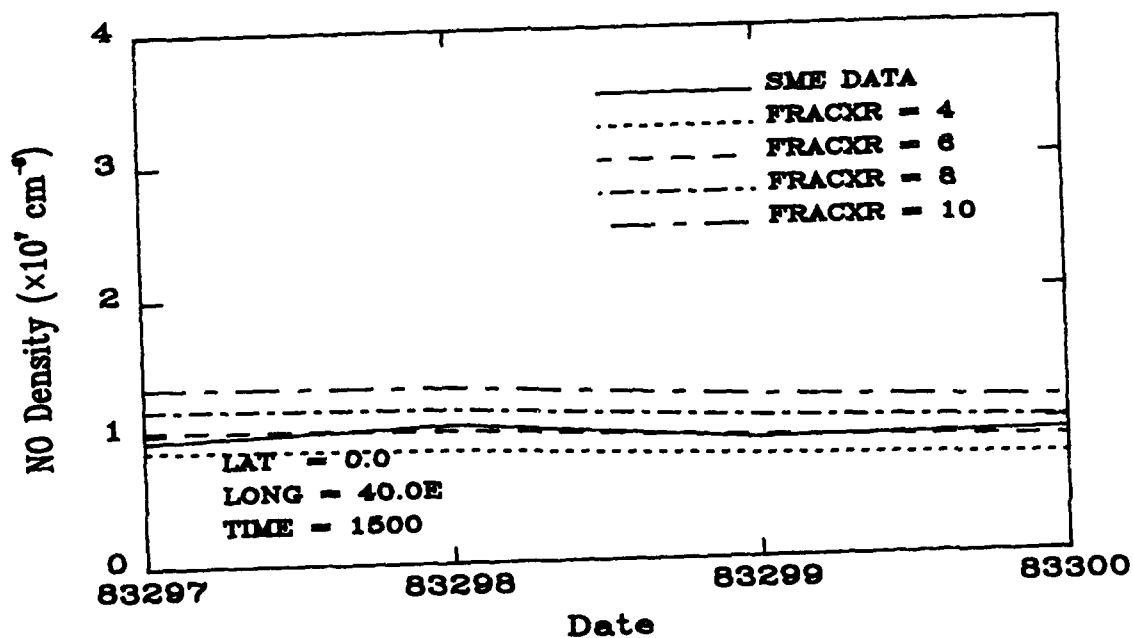

Figure 5.5. Model [NO] densities for F10.7 = 90.
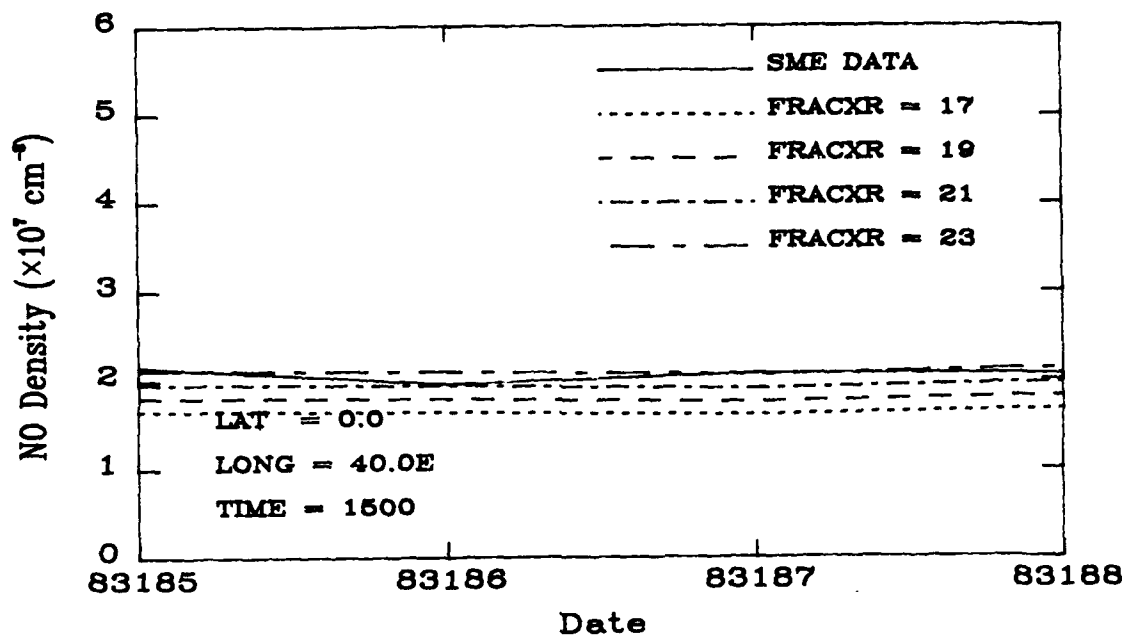
37

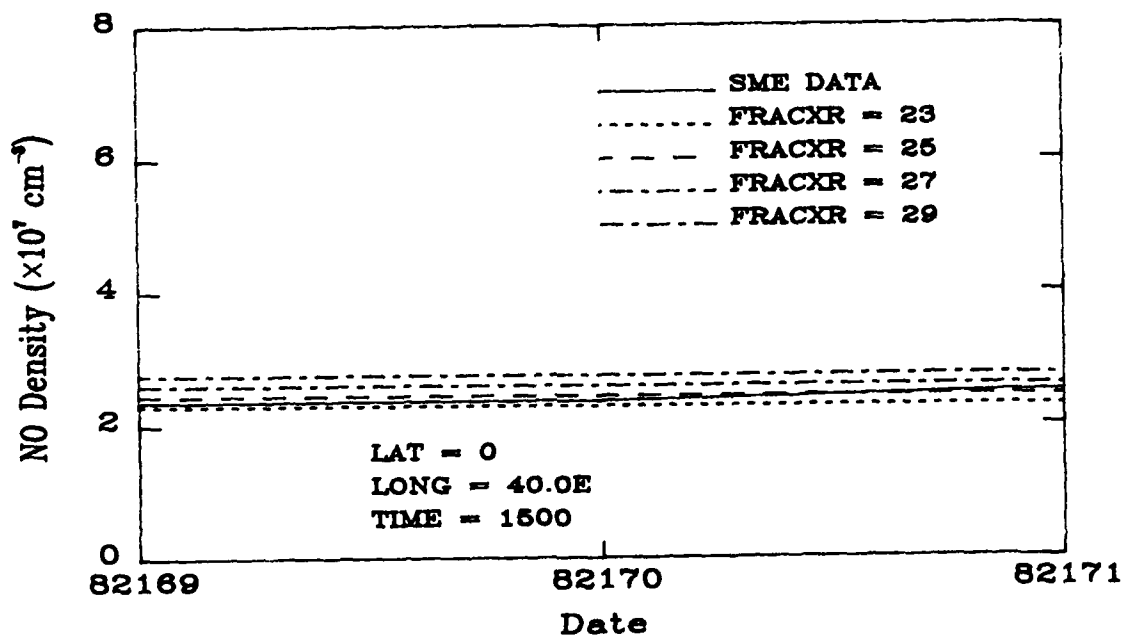Figure 5.6.   Model [NO] densities for F10.7 = 128.

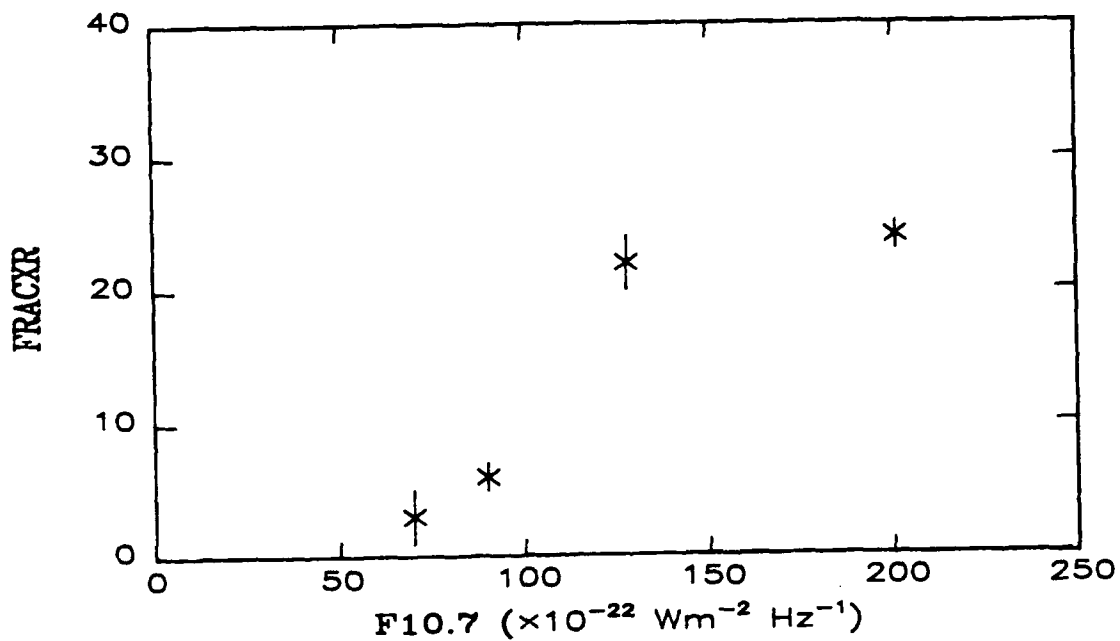Figure 5.7.   Model [NO] densities for F10.7 = 201.
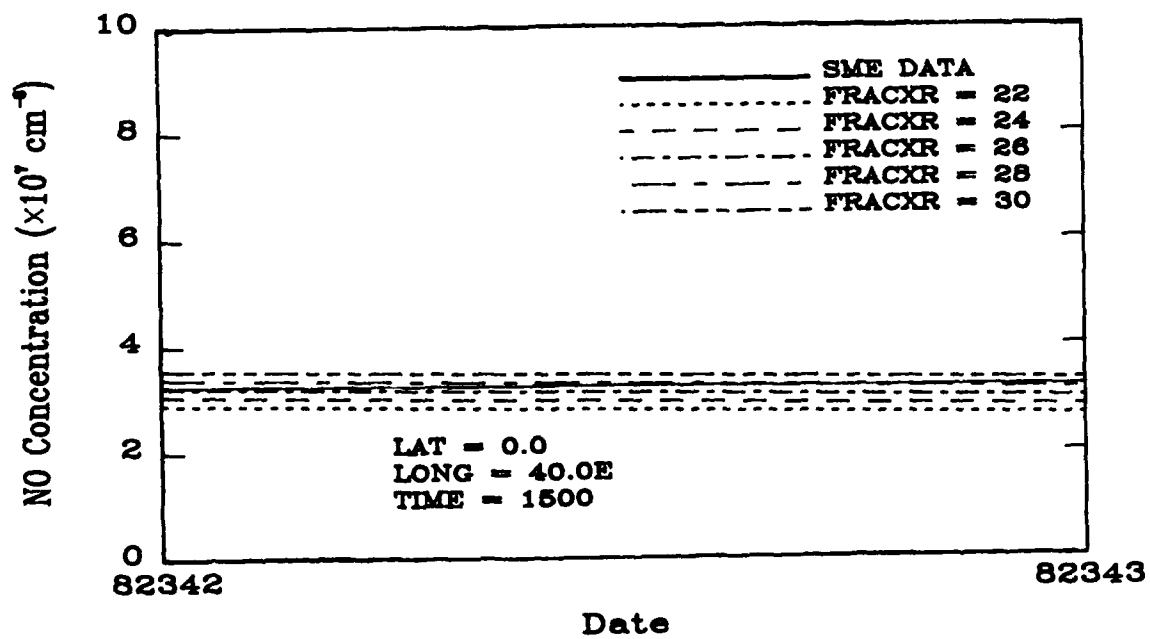
Figure 5.8.   Initial FRACXR Data.

Figure 5.9.   Model [NO] densities for F10.7 = 242

3. Fitting the Data

The addition of the fifth data point at F10.7 = 242
is reflected in Table III, a summary of the final FRACXR
data. The problem now is to find a function (or combination
of functions) which best fits the data. This function can
then be used to determine the value of FRACXR on a daily
basis for input to the model.

TABLE III			
SUMMARY OF FINAL FRACXR DATA			
DATE		F10.7	
START	END	$(\times 10^{-22} \ Wm^{-2}Hz^{-1})$	FRACXR
84300	84303	70	3 ± 2
83297	83300	90	6 ± 1
83185	83188	128	22 ± 2
82169	82171	201	24 ± 1
82342	82343	242	27 ± 1

Several fitting functions were tested. The criteria
for determining the best fit was that function which
minimized χ^2 and was monotonically increasing in FRACXR.
"The definition of χ^2 as the ratio of the estimated variance
s^2 to the parent variance σ^2...makes it a convenient measure
of the goodness of fit." (Bevington, 1969). A weighted
least-squares fit to a third degree polynomial is shown in
Figure 5.10, and a weighted least-squares quadratic fit to

the first four points is shown in Figure 5.11. Weighting
was determined for each data point by

$$w_i = \frac{1}{\sigma_i^2} \, ,$$

where σ_i was taken to be the estimated uncertainty. Figure
5.12 shows a least-squares logarithmic fit, and Figure 5.13
shows a combination of two linear least-squares fits.
Results are summarized in Table IV.

<table>
<tr><td colspan="3" align="center">TABLE IV</td></tr>
<tr><td colspan="3" align="center">SUMMARY OF FITTING FUNCTIONS</td></tr>
<tr><td colspan="2">FUNCTION</td><td>χ^2</td></tr>
<tr><td>THIRD DEGREE POLYNOMIAL</td><td></td><td>10.894</td></tr>
<tr><td>QUADRATIC</td><td></td><td>8.392</td></tr>
<tr><td>LOGARITHMIC</td><td></td><td>87.632</td></tr>
<tr><td>DOUBLE LINEAR</td><td>FIRST LEG
SECOND LEG</td><td>3.951
0.749</td></tr>
</table>
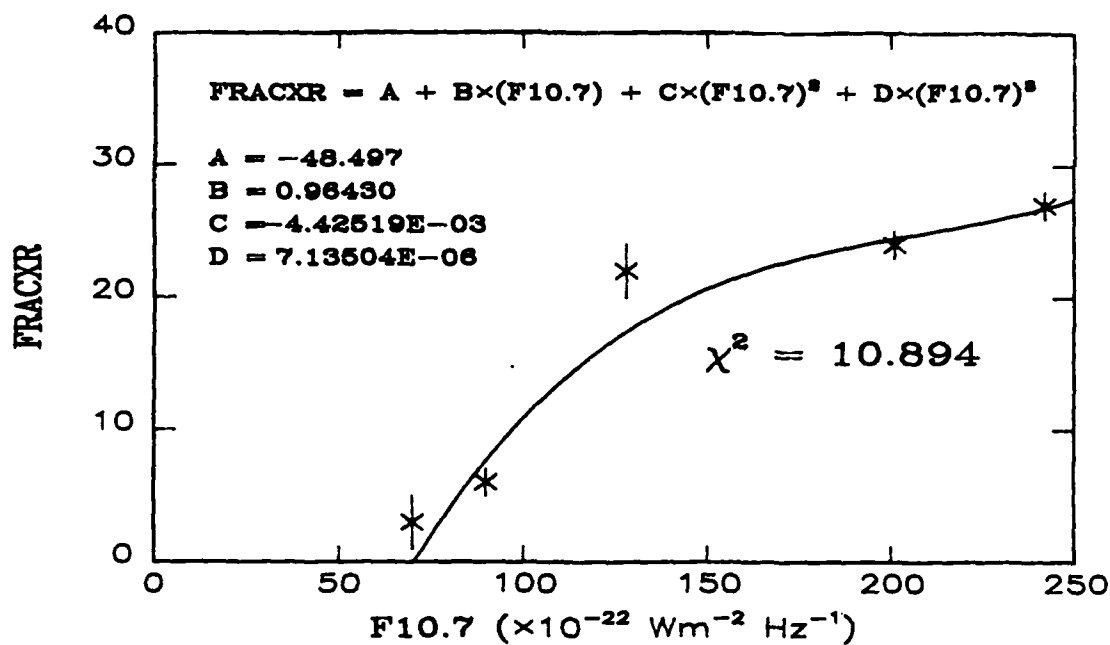
Figure 5.10.   Weighted Third Degree Polynomial Fit.

Chart content:
$FRACXR = A + B \times (F10.7) + C \times (F10.7)^2 + D \times (F10.7)^3$

$A = -48.497$
$B = 0.96430$
$C = -4.42519E{-}03$
$D = 7.13504E{-}06$

$\chi^2 = 10.894$

F10.7 ($\times 10^{-22}$ Wm^{-2} Hz^{-1})
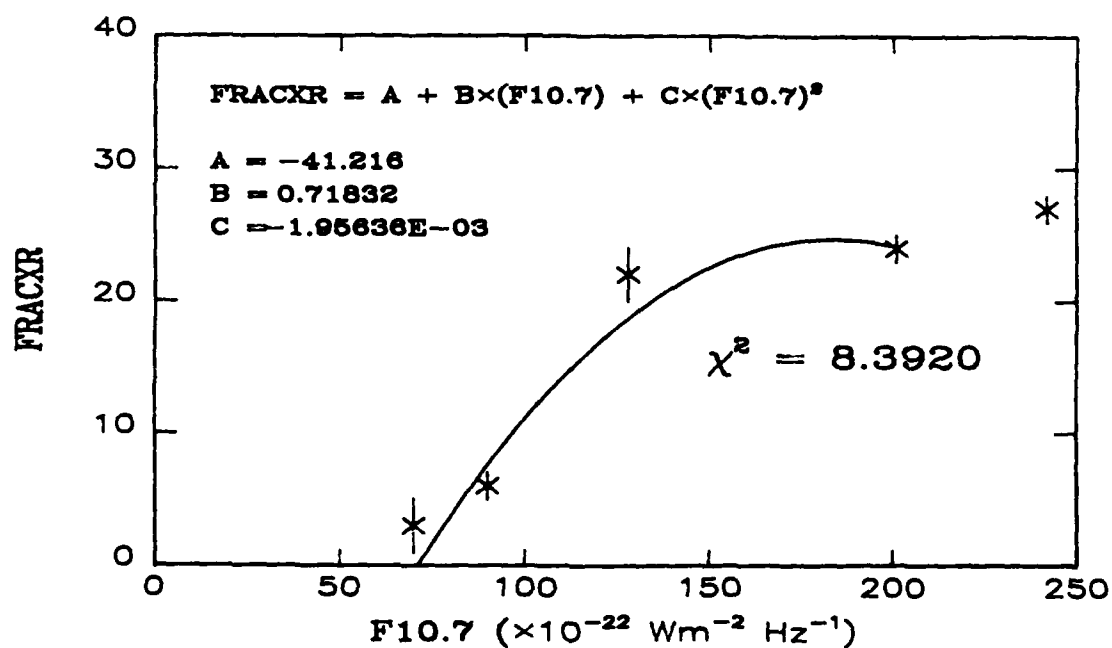
Figure 5.11.   Weighted Quadratic Fit.

Chart content:
$FRACXR = A + B \times (F10.7) + C \times (F10.7)^2$

$A = -41.216$
$B = 0.71832$
$C = -1.95636E{-}03$

$\chi^2 = 8.3920$

F10.7 ($\times 10^{-22}$ Wm^{-2} Hz^{-1})

42

$$FRACXR = A \times \ln \frac{F10.7 - 67}{B}$$

A = 9.8549

B = 12.789

$\chi^2 = 87.632$
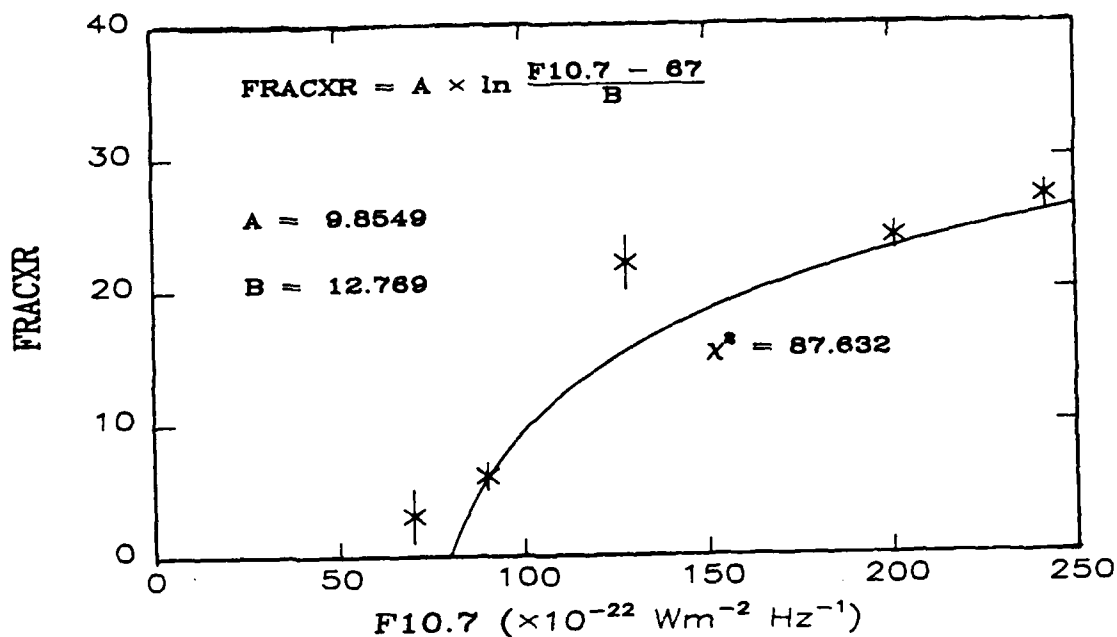
Figure 5.12. Weighted Logarithmic Fit.

FRACXR = A + B×(F10.7)
A =   14.930
B = 4.82255E-02

$\chi^2 = 0.74929$

$\chi^2 = 3.9512$

FRACXR = A + B×(F10.7)
A = -24.513
B = 0.35140
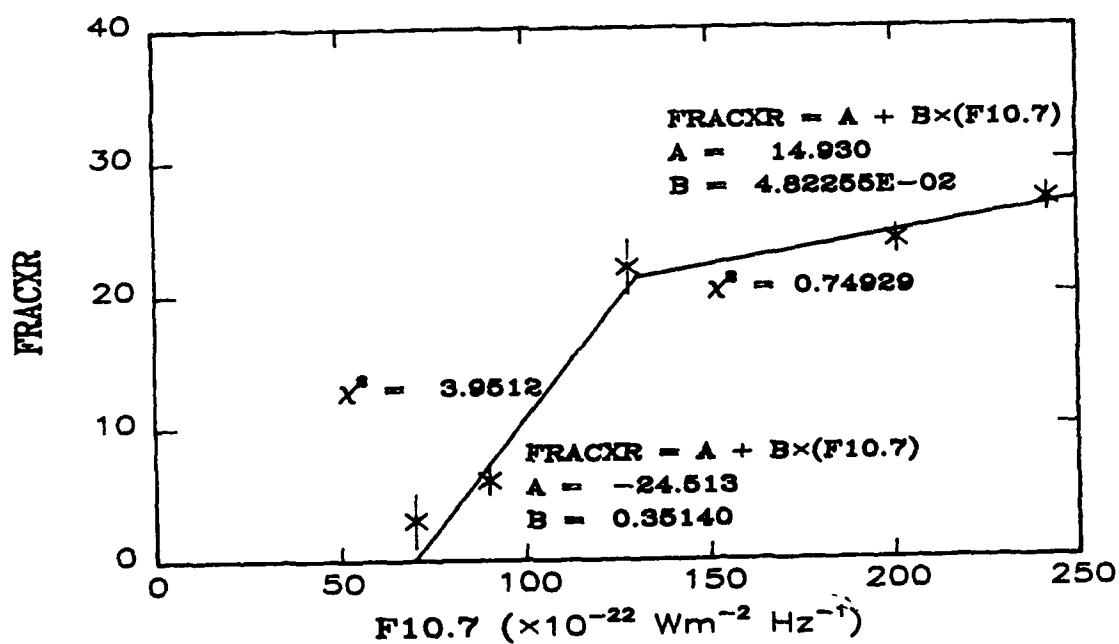
Figure 5.13. Weighted Double Linear Fit.

4. Statement of Empirical Relationship

Based on the results of the analysis presented in the preceding section, the empirical formula for the scaling factor FRACXR which relates X-ray flux and EUV flux in the E-region of the ionosphere is

$$FRACXR = 14.930 + 0.048 \times (F10.7)$$

for F10.7 > 130 and

$$FRACXR = -24.513 + 0.351 \times (F10.7)$$

for F10.7 $\leq$ 130, where F10.7 has units 10^{-22} Wm^{-2} Hz^{-1}.

VI. RESULTS

In Chapter V, an empirical expression for FRACXR was proposed. In this chapter, the expression is incorporated into the one dimensional diffusive photochemical model to compute nitric oxide for two 60 day time periods.

A. COMPARISON OF MODEL AND SME DATA

Two 60 day periods were chosen to further test the model. Each period was chosen to correspond to a time where the SME data showed distinct periodic variations in nitric oxide density. The first 60 day period was from 82213 to 82273, and was chosen because the F10.7 value ($\times 10^{-22}$ W m^{-2} Hz^{-1}) ranged from a minimum of 120 to a maximum of 214 and thus would correspond to FRACXR values taken from the upper curve of Figure 5.13. The result of this 60 day run as well as the daily value for F10.7 is shown in Figure 6.1. Model calculations without using X-ray scaling are included for comparison. The second 60 day period was from 84210 to 84180 , and was chosen because the F10.7 value ($\times 10^{-22}$ W m^{-2} Hz^{-1}) ranged from a minimum of 90 to a maximum of 183 and thus would correspond to FRACXR values taken from the lower curve of Figure 5.13. The result of this 60 day run, along with the F10.7 values and unscaled model calculations, is shown in Figure 6.2.
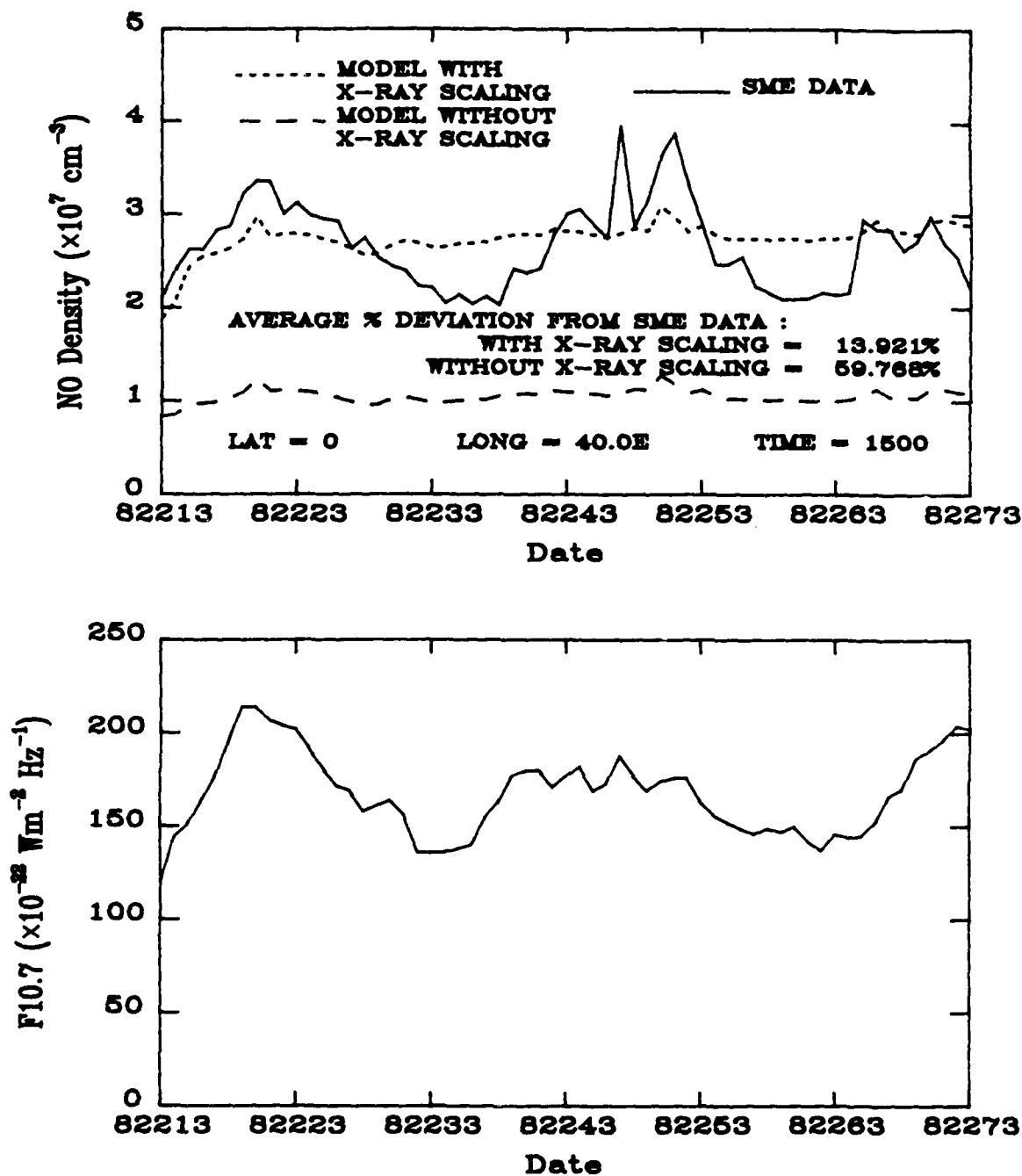
Figure 6.1.   Comparison of SME Data to Model
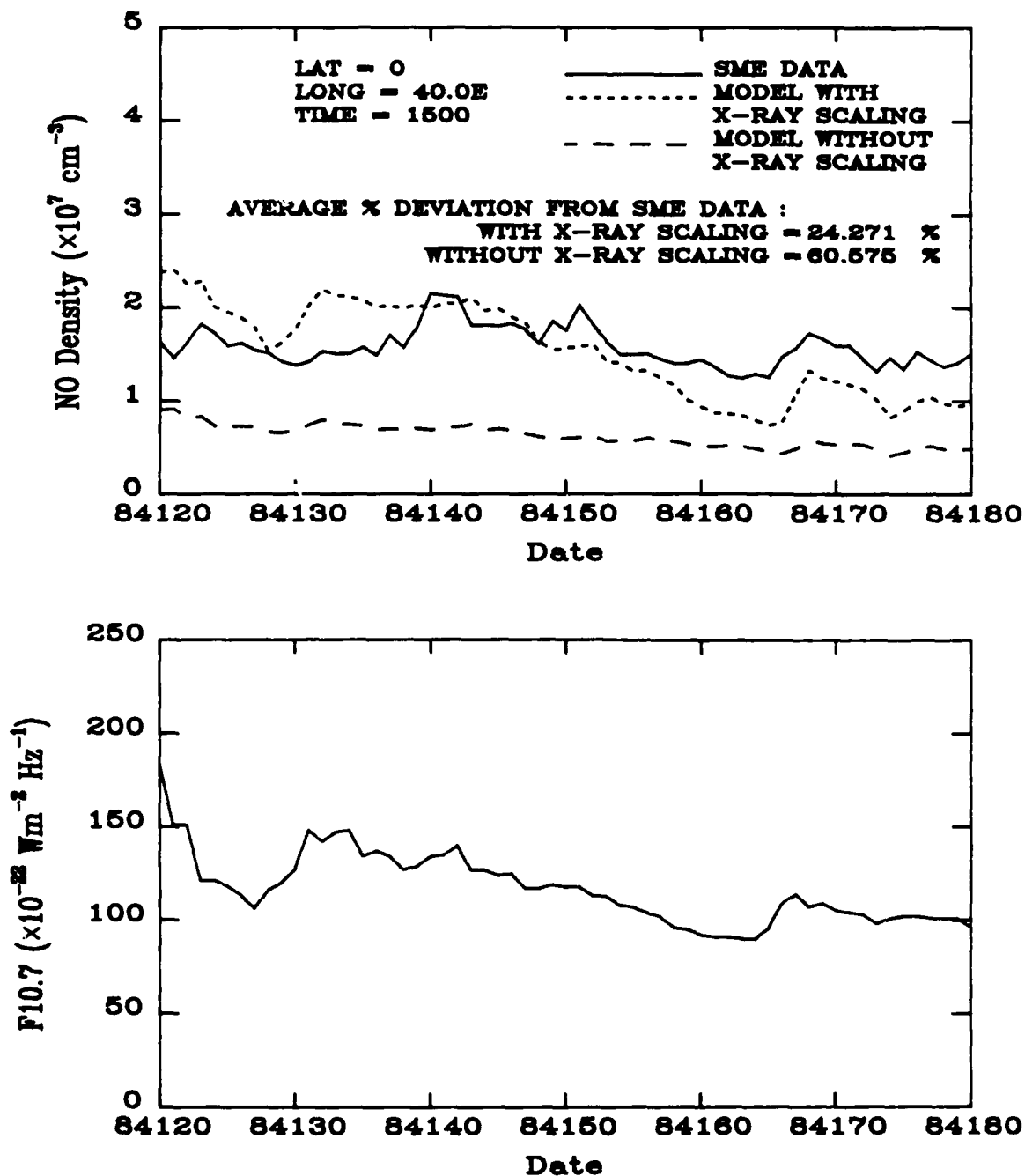for Period of Solar Maximum.

Figure 6.2. Comparison of SME Data to Model
for Period of Solar Minimum.

47

1. Discussion of Results

The average daily deviation of the model calculations for nitric oxide density from the SME satellite measurements was 13.92% for the first 60 day run and 24.27% for the second 60 day run. This is not surprising, since the first run was based on a FRACXR relationship which has a 38% probability of being the correct function ($\chi^2 = .75$), while the second run was based primarily on a FRACXR relationship which only has a 4.8% probability of being the correct function ($\chi^2 = 3.95$). Figures 6.1 and 6.2 show that variations of X-ray flux by a factor of about 30 over the solar cycle can explain the observed variation in nitric oxide density.

Calculated nitric oxide densities for both 60 day runs are plotted against F10.7 to test the correlation between the two data sets in Figure 6.3. An inspection of the figure shows that correlation does exist and follows the same "double linear" type of relation as exists between FRACXR and F10.7. A least-squares fit to each branch of this scatter plot yields lines with regression coefficients of 0.55 and 0.90 for the upper (F10.7 greater than 130) and lower (F10.7 less than 130) parts, respectively. This strongly suggests that FRACXR is incorrectly calculated for values of F10.7 greater than 130.

An inspection of Figures 6.1 and 6.2 reveals that the derived relationship between FRACXR and F10.7 does not
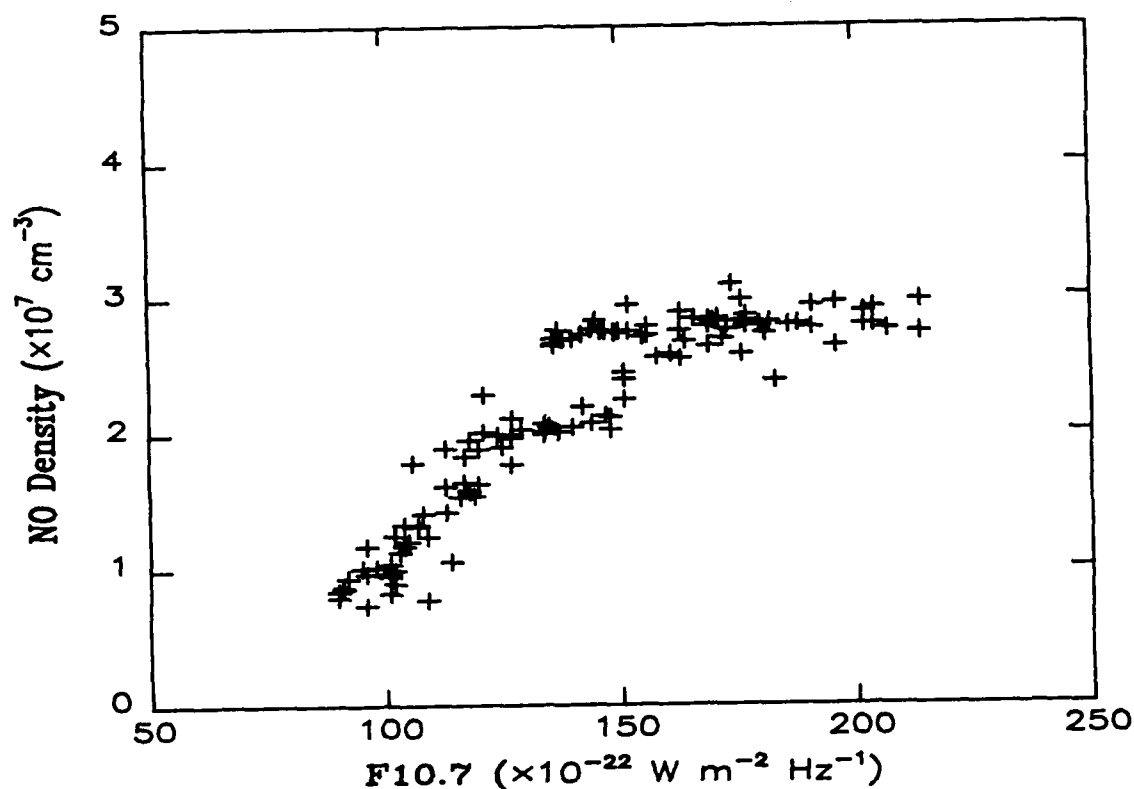
Figure 6.3. Correlation of Calculated NO
Densities and F10.7.

the model to correctly calculate NO densities for values of
F10.7 $(\times 10^{-22}$ W m^{-2} Hz$^{-1})$ from about 140 to 160. The
computed NO densities for these values are too high due to
the artificially high production rate of N(^{2}D) from the
increased X-ray flux. This suggests that a smoother
transition exists between the lower and upper curves of
Figure 5.13 than proposed by the "double linear" fit.

VII. CONCLUSION

A. SUMMARY

A theoretical and observational study of the production of nitric oxide in the E-region of the ionosphere has been presented. The observational basis was the NO measurements made by the Solar Mesosphere Explorer satellite. An empirical expression for the variation in soft solar x-ray flux as a function of the 10.7 cm solar flux was determined. This variation was in the form of a multiplicative scaling factor, FRACXR, between X-ray and EUV flux given by

$$FRACXR = 14.930 + 0.048 \times (F10.7)$$

for F10.7 greater than 130 and

$$FRACXR = -24.513 + 0.351 \times (F10.7)$$

for F10.7 less than or equal to 130, where F10.7 has units 10^{-22} Wm^{-2} Hz^{-1}. The 10.7 cm flux was chosen as the independent parameter because it is used in the neutral atmosphere model as an indicator of solar EUV radiation.

The expression which calculates FRACXR was incorporated into a one dimensional diffusive photochemical model to compute nitric oxide densities. Model calculations for NO densities showed significant improvement in both magnitude and variation. These model calculations were compared to observational measurements from the SME satellite. Results

50

of this comparison showed that model calculations using the above X-ray scaling factor were in much better agreement with the observed SME data than the calculations made without X-ray scaling. The conclusion from this investigation is that variations of soft solar X-ray flux by a factor of 30 over the solar cycle can explain the observed variation in nitric oxide densities.

B. SUGGESTIONS FOR FURTHER RESEARCH

Figure 7.1 shows a scatter plot of observed nitric oxide densities versus 10.7 cm solar flux. Barth et al. (1988) pointed out that the observed nitric oxide densities show a strong correlation with Lyman-α flux over solar cycle. This is shown in Figure 7.2. Examination of these two figures suggests a stronger correlation of NO density to Lyman-α than to F10.7. It is suggested that further investigations be made into model calculations of NO density based on an X-ray scaling factor which is a function of Lyman-α.
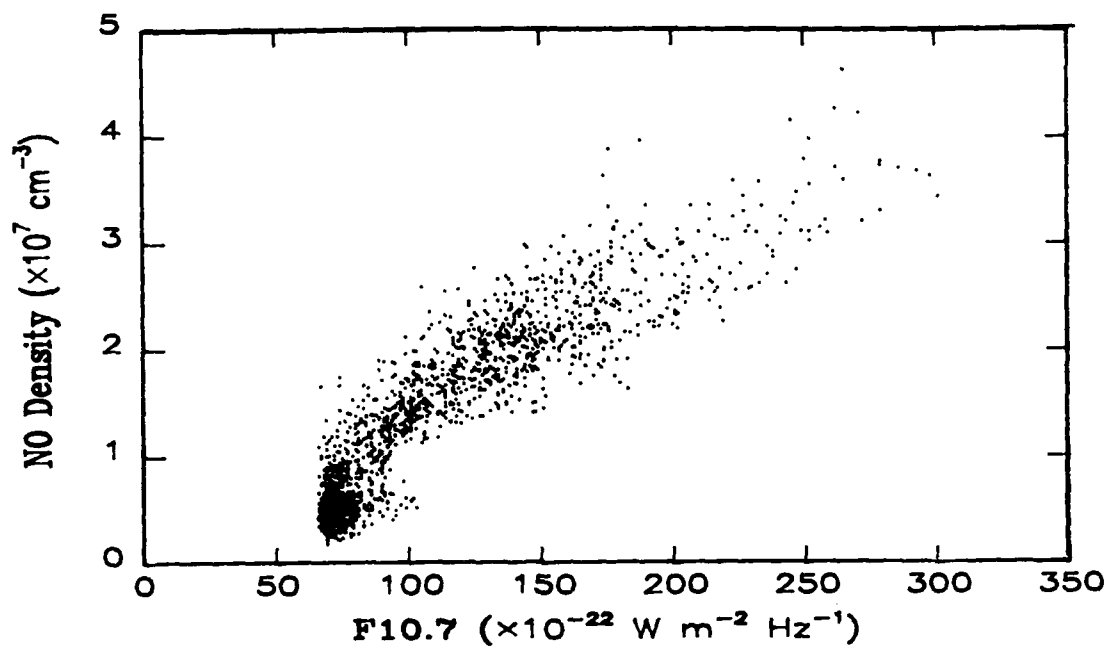
Figure 7.1.   Correlation of NO and F10.7.
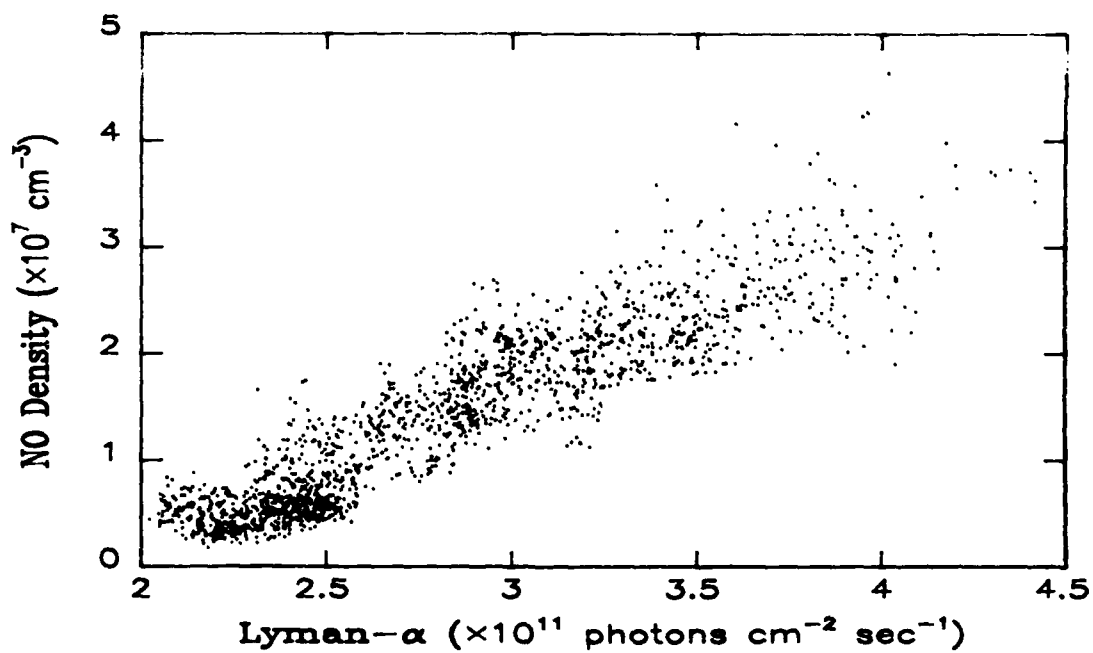
Figure 7.2.   Correlation of NO and Lyman-α.

NITRIC OXIDE REACTIONS IN THE LOWER THERMOSPHERE

This appendix lists all of the reactions used in the Cleary one dimensional photochemical model (1985). Reactions between neutral species are listed first, followed by ion-neutral reactions. Equation numbers shown here reflect the scheme used in Cleary (1986), except for R39 which was added later.

A. NEUTRAL SPECIES

1. Photoionization
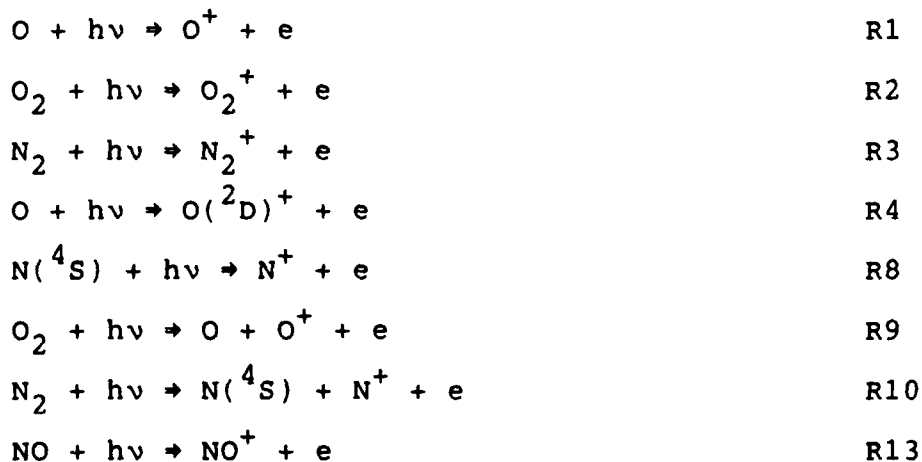
$$O + h\nu \rightarrow O^+ + e \qquad\qquad\qquad\text{R1}$$

$$O_2 + h\nu \rightarrow O_2^+ + e \qquad\qquad\qquad\text{R2}$$

$$N_2 + h\nu \rightarrow N_2^+ + e \qquad\qquad\qquad\text{R3}$$

$$O + h\nu \rightarrow O(^2D)^+ + e \qquad\qquad\qquad\text{R4}$$

$$N(^4S) + h\nu \rightarrow N^+ + e \qquad\qquad\qquad\text{R8}$$

$$O_2 + h\nu \rightarrow O + O^+ + e \qquad\qquad\qquad\text{R9}$$

$$N_2 + h\nu \rightarrow N(^4S) + N^+ + e \qquad\qquad\qquad\text{R10}$$

$$NO + h\nu \rightarrow NO^+ + e \qquad\qquad\qquad\text{R13}$$

2. Photodissociation

$$N_2 + h\nu \rightarrow N(^4S) + N(^4S) \qquad\qquad\qquad\text{R14}$$

$$N_2 + h\nu \rightarrow N(^2D) + N(^2D) \qquad\qquad\qquad\text{R15}$$

$$NO + h\nu \rightarrow O + N(^4S) \qquad\qquad\qquad\text{R16}$$

3. Radiative Relaxation

$$N(^2D) \to N(^4S) + h\nu \qquad\qquad R32$$

4. Quenching

$$N(^2D) + e \to N(^4S) + e \qquad\qquad R30$$

$$N(^2D) + O \to N(^4S) + O \qquad\qquad R31$$

5. Bimolecular Reaction

$$N(^4S) + O_2 \to NO + O \qquad\qquad R28$$

$$N(^2D) + O_2 \to NO + O \qquad\qquad R29$$

$$N(^2P) + O_2 \to NO + O \qquad\qquad R39$$

$$N(^4S) + NO \to N_2 + O \qquad\qquad R33$$

$$N(^2D) + NO \to N_2 + O \qquad\qquad R34$$
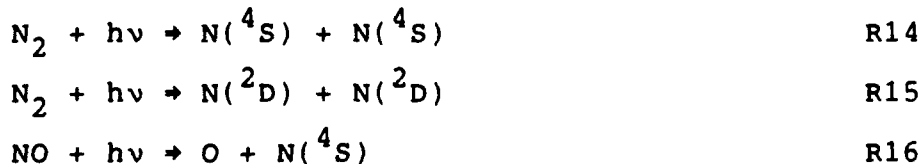
6. Energy Transfer or Photoelectron Impact
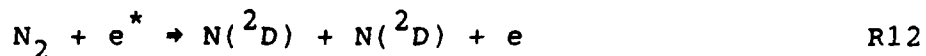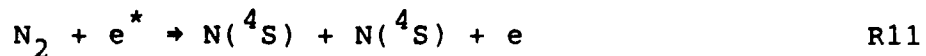
$$O + e^* \to O^+ + 2e \qquad\qquad R5$$

$$O_2 + e^* \to O_2^+ + 2e \qquad\qquad R6$$

$$N_2 + e^* \to N_2^+ + 2e \qquad\qquad R7$$

$$N_2 + e^* \to N(^4S) + N(^4S) + e \qquad\qquad R11$$

$$N_2 + e^* \to N(^2D) + N(^2D) + e \qquad\qquad R12$$

B. IONS

1. Charge Transfer

$$N_2^+ + O_2 \to O_2^+ + N_2 \qquad\qquad R18$$

$$O^+ + O_2 \to O_2^+ + O \qquad\qquad R21$$

$$O_2^+ + NO \to NO^+ + O_2 \qquad\qquad R22$$

$$O(^2D)^+ + N_2 \to N_2^+ + O \qquad\qquad R35$$

$$O(^2D)^+ + O_2 \to O_2^+ + O \qquad\qquad R36$$

2. **Ion–Atom Interchange**

$$N_2^+ + O \rightarrow NO^+ + N(^2D) \hspace{4cm} R17$$

$$O^+ + N_2 \rightarrow NO^+ + N(^4S) \hspace{4cm} R20$$

$$O_2^+ + N(^4S) \rightarrow NO^+ + O \hspace{4cm} R23$$

$$N^+ + O_2 \rightarrow NO^+ + O \hspace{4cm} R25$$

3. **Dissociative Recombination**

$$N_2^+ + e \rightarrow N(^2D) + N(^2D) \hspace{3cm} R19$$

$$O_2^+ + e \rightarrow O + O \hspace{4cm} R24$$

$$NO^+ + e \rightarrow O + N(^4S) \hspace{3.5cm} R26$$

$$NO^+ + e \rightarrow O + N(^2D) \hspace{3.5cm} R27$$
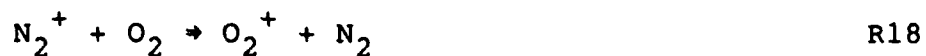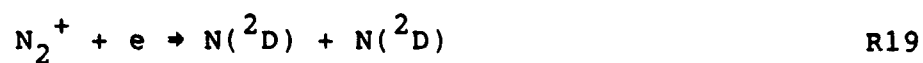
LIST OF REFERENCES

Barth, C.A., Tobiska, W.K., Siskind, D.E., and Cleary, D.D., "Solar-Terrestrial Coupling : Low Latitude Thermospheric Nitric Oxide," Geophysical Research Letters, v. 15, No. 1, pp. 92-94, January 1988.

Bauer, S.J., Physics of Planetary Ionospheres, Springer-Verlag, 1973.

Bevington, R.P., Data Reduction and Error Analysis for the Physical Sciences, McGraw-Hill, Inc., 1969.

Chamberlain, J.W., The Theory of Planetary Atmospheres: An Introduction to Their Physics and Chemistry, Academic Press, Inc., 1978.

Cleary, D.D., Analysis of Nitric Oxide Fluorescence Bands From High Latitude Rocket Observations of the Thermospheric Dayglow, Ph.D. Dissertation, Department of Astrophysical, Planetary and Atmospheric Sciences, University of Colorado, Boulder, Colorado, 1985.

Cleary, D.D., "Daytime High-Latitude Rocket Observations of the NO γ, δ, and ϵ Bands," Journal of Geophysical Research, v. 91, pp. 11337, 1986.

Colgrove, F.D., Johnson, F.S., and Hanson, W.B., "Atmospheric Composition in the Lower Thermosphere," Journal of Geophysical Research, v. 71, pp. 2227-2236, May 1966.

Goody, R.M. and Walker, J.C.G., Atmospheres, Prentice-Hall, Inc., 1972.

Hedin, A.E., "A Revised Thermospheric Model Bases on Mass Spectrometer and Incoherent Scatter Data: MSIS-83," Journal of Geophysical Research, v. 88, pp. 10170-10188, December 1983.

Heiklen, J., Atmospheric Chemistry, Academic Press, Inc., 1976.

Hickman, D.R., Morse, F.A., and Pranke, J.B., "Remote Sensing of the Neutral Constituents of the Lower Thermosphere," NATO Advanced Study Institute on the Dynamical and Chemical Coupling of the Neutral and Ionized Atmosphere, B. Grandal and J.A. Holtet (eds.), pp. 73-78, D. Reidel Publishing Company, Dordrecht, Holland, 1977.

Liou, K., An Introduction to Atmospheric Radiation, Academic Press, Inc., 1980.

McEwan, M.J. and Phillips, L.F., Chemistry of the Atmosphere, Halsted Press, 1975.

National Oceanographic and Atmospheric Administration, NOAA-S/T76-1562. U.S. Standard Atmosphere (1976). Superintendent of Documents, U.S. Government Printing Office, Washington, DC.

Naval Research Laboratory Memorandum Report 5004, Photoelectron Model for the Rapid Computation of Atmospheric Excitation Rates, by D.J. Strickland and R.R. Meier, 1982.

Siskind, D.E., The Response of Thermospheric Nitric Oxide to an Auroral Storm, Ph.D. Dissertation, Department of Astrophysical, Planetary and Atmospheric Sciences, University of Colorado, Boulder, Colorado, 1988.

Shimazaki, T., Minor Constituents in the Middle Atmosphere, Terra Scientific Publishing Company, 1985.

Telephone conversation between David E. Siskind, University of Michigan, Ann Arbor, Michigan, and the author, 9 November 1988.

Telephone conversation between Dr. Charles A. Barth, Laboratory for Atmospheric and Space Physics, University of Colorado, Boulder, Colorado, and the author, 17 November 1988.

Torr, M.R., Torr, D.G., Ong, R.A. and Hinteregger, H.E., "Ionization Frequencies for Major Thermospheric Constituents as a Function of Solar Cycle 21," Geophysical Research Letters, v. 6, pp. 771-774, October 1979.

Von Rosenberg, D.U., Methods for the Numerical Solution of Partial Differential Equations, American Elsevier, New York, 1969

Wallace, J.M. and Hobbs, P.J., Atmospheric Science: An Introductory Survey, Academic Press, Inc., 1977.

INITIAL DISTRIBUTION LIST

1. Defense Technical Information Center   2
   Cameron Station
   Alexandria, Virginia 22304-6145

2. Library, Code 0142   2
   Naval Postgraduate School
   Monterey, California 93943-5002

3. Dr. K. Woehler, Chairman   1
   Physics Department
   Naval Postgraduate School
   Monterey, California 93943-5000

4. Dr. David D. Cleary   5
   Physics Department, 61-Cl
   Naval Postgraduate School
   Monterey, California 93943-5000

5. Dr. S. Gnanalingam   1
   Physics Department, 61-Gm
   Naval Postgraduate School
   Monterey, California 93943-5000

6. Dr. Charles A. Barth   1
   Laboratory for Atmospheric and Space Physics
   University of Colorado
   Boulder, Colorado 80309-0392

7. Dr. Robert McCoy   1
   Code 4140
   Naval Research Laboratory
   Washington D.C. 20375

8. LT Richard A. Dumas, USN   1
   Department Head School Class 107
   Surface Warfare Officers School Command
   Newport, Rhode Island 02841-5012